

AD-A068 582

COLD REGIONS RESEARCH AND ENGINEERING LAB HANOVER NH  
COMPUTER MODELING OF ATMOSPHERIC ICE ACCRETION, (U)

F/G 8/12

MAR 79 S F ACKLEY, M K TEMPLETON

UNCLASSIFIED

CRREL-79-4

NL

| OF |  
AD  
AO 582

END  
DATE  
FILED  
6 - 79  
DDC

**CRREL** LEVEL 12

**REPORT 79-4**



*Computer modeling of atmospheric  
ice accretion*

AD A068582

DDC FILE COPY



*For conversion of SI metric units to U.S./British customary units of measurement consult ASTM Standard E380, Metric Practice Guide, published by the American Society for Testing and Materials, 1916 Race St., Philadelphia, Pa. 19103.*

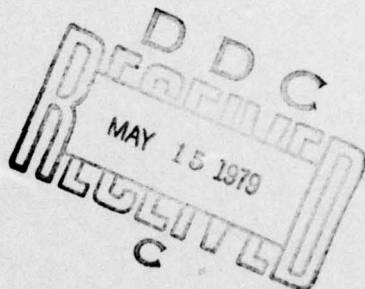
*Cover: Accretion of rime ice, formed from sub-freezing cloud droplets, on a suspended cable on the summit of Mt. Washington, New Hampshire, in April 1978. The cable was instrumented to measure the additional loading placed on it by wind and gravity forces acting on the attached ice. (Photograph by Jon Lingel, Mt. Washington Observatory.)*

# CRREL Report 79-4



## *Computer modeling of atmospheric ice accretion*

S.F. Ackley and M.K. Templeton



Prepared for  
**DIRECTORATE OF MILITARY PROGRAMS**  
**OFFICE, CHIEF OF ENGINEERS**  
By  
**UNITED STATES ARMY**  
**CORPS OF ENGINEERS**  
**COLD REGIONS RESEARCH AND ENGINEERING LABORATORY**  
**HANOVER, NEW HAMPSHIRE, U.S.A.**

Unclassified

SECURITY CLASSIFICATION OF THIS PAGE (When Data Entered)

REPORT DOCUMENTATION PAGE		READ INSTRUCTIONS BEFORE COMPLETING FORM
1. REPORT NUMBER 14 CRREL Report 79-4	2. GOVT ACCESSION NO.	3. RECIPIENT'S CATALOG NUMBER
4. TITLE (and Subtitle) 6 COMPUTER MODELING OF ATMOSPHERIC ICE ACCRETION		5. TYPE OF REPORT & PERIOD COVERED
7. AUTHOR(s) 10 S.F./Ackley and M.K./Templeton		6. PERFORMING ORG. REPORT NUMBER 16
9. PERFORMING ORGANIZATION NAME AND ADDRESS U.S. Army Cold Regions Research and Engineering Laboratory Hanover, New Hampshire 03755		10. PROGRAM ELEMENT, PROJECT, TASK AREA & WORK UNIT NUMBERS DA Project 4A161102AT24 DA Project 4A7670AT42
11. CONTROLLING OFFICE NAME AND ADDRESS Directorate of Military Programs Office, Chief of Engineers Washington, D.C. 20314		11. REPORT DATE 11 March 79
14. MONITORING AGENCY NAME & ADDRESS (if different from Controlling Office) 980		12. NUMBER OF PAGES 39 1241 p.
15. SECURITY CLASS. (of this report) Unclassified		
15a. DECLASSIFICATION/DOWNGRADING SCHEDULE		
16. DISTRIBUTION STATEMENT (of this Report) Approved for public release; distribution unlimited.		
17. DISTRIBUTION STATEMENT (of the abstract entered in Block 20, if different from Report)		
18. SUPPLEMENTARY NOTES		
19. KEY WORDS (Continue on reverse side if necessary and identify by block number) Cold regions Ice Computerized simulation Ice formation Control Mathematical models Deicing systems Test methods Drops Clouds		
20. ABSTRACT (Continue on reverse side if necessary and identify by block number) A computer model is described to compute the amount of ice accretion on an object under a variety of initial conditions. Numerical techniques are best applied to these problems because of time dependent effects governing the amount of ice collected and also the variety of initial conditions that can lead to ice accumulation. The helicopter rotor icing problem adds an additional complexity since the velocity along the rotor blade varies over a wide range strongly affecting the amounts of ice collected at different blade positions. The physics of ice accretion is reviewed and the accounting for time-dependence in the computer model is described. Some model results are presented and indicate the dependence of ice accretion on velocity, droplet sizes, cloud liquid water content, and temperature for a cylindrical object of constant size.		

## PREFACE

This report was prepared by S.F. Ackley, Research Physicist, Snow and Ice Branch, Research Division and M.K. Templeton, Math Aide, Snow and Ice Branch (now at California Institute of Technology).

The study was conducted under DA Project 4A161102AT24, *Adhesion and Physics of Ice* and DA Project 4A1670AT42, *Prevention and Control of Ice Adhesion*.

Mr. Walter B. Tucker III and Mr. L. David Minsk reviewed the technical content of this report.

The authors wish to thank Dr. G. Ashton, Chief, Snow and Ice Branch and Program Manager for CRREL's Ice Adhesion Program for his continued support and encouragement of this work.

ACCESSION for	
NTIS	White Fiction <input checked="" type="checkbox"/>
DDC	S. I. Section <input type="checkbox"/>
UNAMERIC	<input type="checkbox"/>
JUS	<input type="checkbox"/>
BY	
DISTRIBED BY/AVAILABILITY CODES	
SPECIAL	
X	

## CONTENTS

	Page
<b>Abstract</b> .....	i
<b>Preface</b> .....	ii
<b>Introduction</b> .....	1
<b>Ice accretion parameters</b> .....	2
<b>Physics of ice accretion</b> .....	2
1. Interaction between water droplets and flow field.....	2
2. Time dependence in droplet trajectories.....	4
3. Thermodynamic processes at the surface of the object .....	4
4. Time dependence in the thermodynamics .....	6
5. Time dependence of lesser order.....	6
<b>Numerical ice accretion model</b> .....	7
1. Major subroutines.....	7
2. Options for droplet size variations .....	11
3. Option for the helicopter rotor case .....	15
<b>Results</b> .....	16
<b>Conclusions and future studies</b> .....	20
<b>Literature cited</b> .....	21
<b>Appendix A: Computer program</b> .....	23

## ILLUSTRATIONS

### Figure

1. Velocity potential $\phi$ and stream function $\psi$ around a circular cylinder of radius $a$ em- bedded in a fluid with free stream velocity $u$ .....	3
2. Air streamlines and droplet trajectories with respect to a right circular cylinder.....	4
3. Schematic indicating the five terms used in the heat balance and whether they are carrying heat toward or away from the freezing surface.....	6
4. The fraction of accreted water lost for various temperatures and average radii of accret- ing objects.....	7
5. Block diagram of the numerical model for calculating ice accretion .....	8
6. Initial variables input in the run control sequence of the numerical model .....	8
7. Subroutines Profile and Ice Den used to calculate the changes in object profile and ice density from the output of the icing thermodynamics .....	9
8. Subroutines controlling computation of the droplet trajectory, collection efficiency and trajectory control, and free stream velocity.....	10
9. Based on the ambient conditions, the calculation of mass accreted is completed by in- corporating the thermodynamics at the surface.....	13
10. Forms of the Erlang distribution for various values of the parameter $k$ .....	14
11. (Top) The change in profile dimension at 50-s intervals by ice accretion..... (Bottom) The surface temperature of the front half cylinder as a function of time.....	15
12. Numerical simulation of helicopter rotor blade icing showing the surface temperature, leading edge ice thickness, collection efficiency and fraction accreted as a function of velocity for the initial conditions shown.....	16
13. Droplet trajectories and ice profile changes for a Gaussian droplet size distribution .....	17
14. Accreted ice thickness and temperature for the ambient conditions indicated .....	18
15. Comparison between experimental data and model simulation of the same conditions.....	19
16. Magnitude of the individual thermodynamic terms as a function of velocity for the simu- lation shown in Figure 12.....	20

# COMPUTER MODELING OF ATMOSPHERIC ICE ACCRETION

S.F. Ackley and M.K. Templeton

## INTRODUCTION

Work on ice accretion from the atmosphere has followed two distinct lines, hailstone growth and aircraft icing. Most recently, investigations of hailstone growth have provided the justification for a general understanding of ice accretion processes. The concept is that damaging hail grows in several regions within convective cumulus clouds. Through examination of the structure of hailstones, information on the ambient conditions within the clouds can be obtained, specifically liquid water content ( $lwc$ ), droplet radius ( $R_{drop}$ ) and air temperature ( $T_0$ ). The hailstones can then be used to interpret and model cloud structures, and possibly to provide information on structure modification by cloud-seeding methods for preventing and slowing down hail growth. Macklin et al. (1976, 1977), List et al. (1971), and Knight and Knight (1968) provided the conceptual background for this application and described several recent efforts to obtain this information.

Early ice accretion work (e.g. Langmuir and Blodgett 1946) emphasized its application to airplane icing. Icing loads affected aircraft performance, making it necessary to provide ice detection and deicing systems (Tribus 1943, Messinger 1953). As aircraft evolved to types that flew higher and faster, however, research in this area declined, since major icing problems occur at altitudes below 20,000 ft (6100 m) and at air speeds below 300 mph (134 m/s), primarily in clouds ranging from about 0 to  $-20^{\circ}\text{C}$  in temperature. The faster and higher flying commercial and military planes of today pass quickly through these conditions. Jet aircraft also have power available to overcome icing on engine intakes and other critical areas by heating, so recent efforts have been directed toward finding engineering solutions to typical or worst cases rather than toward continued research into the physics of the ice accretion process.

The fundamental physics indicated that particular cases could be formulated, but that the computations necessary to give a complete analysis were complex. For example, cumbersome analog devices requiring several persons working simultaneously were necessary

to obtain the initial water droplet trajectories of impact. These initial trajectories were, of course, only one aspect of the total problem (Brun 1957, Langmuir and Blodgett 1946).

Research on helicopters and the possibility of making them capable of operation in any weather, including icing conditions, has proceeded sporadically but with continued interest since helicopter flight is limited mainly to the lower altitudes and air speeds where icing is more frequently encountered. Stallabrass (1957, 1958) conducted experiments on helicopters hovering under various icing conditions, using a water spray stand to simulate the icing cloud. Using the formulation developed from earlier aircraft work, he found that the icing accretion rate on the main rotor blades could be simulated by applying the fixed velocity calculation developed by Messinger (1953) for fixed-wing aircraft to each segment along the rotor blade characterized by its velocity:

$$v_i = r_i \omega \quad (1)$$

where  $\omega$  is the angular velocity of the rotor blade and  $r_i$  is the distance from the center of the hub (axis of rotation) to the segment of interest. Good agreement was found between the experimentally obtained ice shapes and those predicted using the calculations from the earlier work on aircraft at a single velocity (Dickey 1952).

The aim of this report is to demonstrate a method for calculating the quantity of ice that will accrete on fixed-wing aircraft, helicopters, ships, power lines, radomes, towers and other structures under a given set of conditions.

Although much of the previous work has been fundamentally correct in formulating the time-dependent process of ice accretion, one of the problems has been the exclusion of time dependence in the application of the formalism. In order to estimate ice accretion mass confidently over a wide range of conditions, the influence of this time dependence must be accounted for.

In this paper, we reexamine the fundamentals of the ice accretion process, and point out those features in

the governing relationships for ice accretion that require special treatment because they implicitly contain time dependence leading to feedback effects. We then show how the time-dependent formalism is solved using numerical methods to more correctly account for these feedback effects, and include them in calculations of ice accretion on objects, given the atmospheric conditions and object parameters. The computer model is useful as a simulation tool to provide input for design purposes, such as aircraft and helicopter deicing design, or ground-based structural applications, such as power line or tower icing prediction, or as a research tool to examine the sensitivity of the icing process to variations in the input variables, either singly or in concert. These simulations may assist in the understanding of limited laboratory and field testing, lending some generality to the ice accretion processes observed there, and extending this information to applications where data are limited, for example, power line icing in remote locations, and helicopter icing in the extreme cases that are currently untested.

## ICE ACCRETION PARAMETERS

Atmospheric ice accretion is caused principally by the freezing of supercooled water droplets. The droplets may freeze after they are carried to a collision with an object by airflow (ground-based structure), or as an object, such as an airplane or helicopter, passes through them. Supercooled water is necessary because ice particles alone do not stick on impact and, therefore, do not cause an ice accretion problem. Recently there have been some indications that mixed clouds, containing both ice particles and supercooled water droplets, can cause a serious ice accretion problem, especially for helicopters (Stallabrass, pers. comm.). This problem ostensibly occurs because the ice particles, in the presence of supercooled water, adhere to the surface of the object, and, because they are already frozen, do not require the heat transfer that an unfrozen droplet of similar size requires to compensate for the large latent heat of freezing. However, icing tunnel tests have indicated that the amount of sticking by ice crystals is lower than expected, indicating that mixed conditions may not be as critical as was first assumed.

In the first case, we will consider only water droplets, since the effects of mixed conditions have not been studied sufficiently to allow a quantitative formulation. The primary sources of icing conditions are clouds and fogs since the smaller droplets present in them can sustain substantial supercooling over a wide temperature

range. Raindrops are larger and therefore cannot undergo the same degree of supercooling (Mason 1971). However, the formulation can be applied to clouds, fog, rain, sea spray, and spray of man-made origin, e.g. power plant cooling tower fog, as long as the correct parameters can be specified. The six parameters necessary for quantifying the problem can be conveniently divided into three properties of the atmosphere—the ambient temperature  $T_0$ , the liquid water content  $w_c$ , and the droplet radius distribution  $R_{\text{drop}}$ —and three of the accreting object—its cross-sectional diameter ( $2a$ ), velocity  $u$  and shape, e.g. cylinder, airfoil, etc. The interaction of these parameters will be identified in the next section.

## PHYSICS OF ICE ACCRETION

If we move an object through a supercooled cloud, the rate of ice accretion depends on two factors. First, it depends on the kinematic interaction between the object and the droplets in the cloud. This relation determines whether particular droplet sizes are captured. Second, it depends on the thermodynamic processes at the surface of the object. Here, a balance is obtained between the rate of heat release necessary to freeze all or part of the impinging water and the rate at which heat can be carried away from the surface into the flow field by the processes of convection, evaporation and radiation. We first consider the kinematic interaction.

### 1. Interaction between water droplets and flow field

Normally, the speeds at which icing occurs are such that the air around the object can be treated as an ideal, incompressible fluid. The velocity field exhibits continuity, and mathematically (Sokolnikoff and Redheffer 1966) satisfies the condition for the application of potential theory (i.e.  $\nabla \times u = 0$ ,  $\nabla \cdot u = 0$ ). The velocity can therefore be solved for at any point around the object by solution of a complex potential of the form:

$$F = \phi + i\psi \quad (2)$$

where  $\phi$  is the velocity potential and  $\psi$  the stream function, and the curves of  $\phi$ ,  $\psi$  are orthogonal functions defining the complex flow field. The velocity of the fluid at any point is given by

$$u_0 = \nabla\phi \quad (3)$$

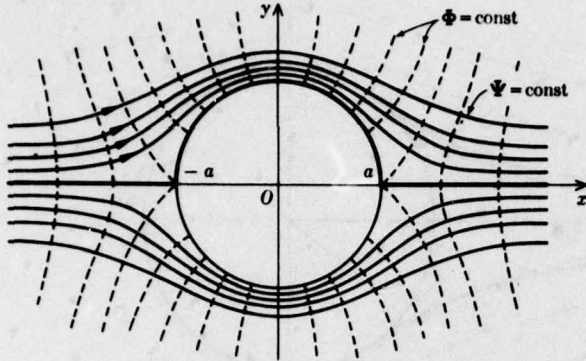


Figure 1. Velocity potential  $\phi$  and stream function  $\psi$  around a circular cylinder of radius  $a$  embedded in a fluid with free stream velocity  $u$ .

Because of the orthogonality between  $\phi$  and  $\psi$ , the velocity is tangent to the curves  $\psi = \text{const}$ . These are the paths or streamlines of the fluid elements. We consider a circular cylinder as an example. Figure 1 shows the streamlines around such a circular cylinder, with flow perpendicular to the long axis. Two consequences of complex potential flow theory are that the boundary of the object coincides with one of the streamlines ( $\psi = \text{const}$ . at the boundary), and the flow satisfies Laplace's equation,  $\nabla^2 F = 0$ , in the entire plane. For objects of simple cross-sectional geometry, such as circles or ellipses, the dimensionless velocity at any point can be determined straightforwardly if we know the free stream velocity  $u$  (i.e. at great distances from the object) and the characteristic dimensions of the object—for the cylinder, its radius  $a$  (Milne-Thomson 1960).

To determine the interaction between the droplets and the flow field, we integrate the equation of motion for the droplet in the flow field. Following Brun (1957), the assumptions for this formulation are: a) the streamlines determined for clear air are valid, i.e. there are not enough droplets to perturb the flow, b) the gravity forces are much less than the inertial forces and may be neglected, c) the pressure forces on a droplet are equivalent to those on an equal volume of air at the same location, and consequently may also be neglected because water has a much greater density than air.

The motion of the droplet, therefore, results primarily from the inertial and viscous drag forces as it drifts with the fluid streamline. The drag force is proportional to the velocity and the drag coefficient  $c_d$  that the droplet sees at any given time. Newton's second law in dimensionless form for the droplet (after Langmuir and Blodgett 1946) therefore becomes, for the circular cylinder case:

$$k \frac{d\bar{u}_d}{dt} = \frac{c_d \text{Re}}{24} (\bar{u}_d - \bar{u}_0). \quad (4)$$

Here  $\bar{u}_d$  is the dimensionless velocity of the droplet at any point,  $\bar{u}_0$  the dimensionless streamline velocity at the same point,  $\text{Re}$  the Reynolds number =  $2R_{\text{drop}} \rho_{\text{air}} [(\bar{u}_d - \bar{u}_0)u] / \mu$ ,  $c_d$  the drag coefficient, and  $k$  the inertial parameter (analogous to mass in dimensionless form) =  $2\rho_w R_{\text{drop}}^2 (u/9\mu a)$ .

The drag coefficient  $c_d$  of a spherical drop is also a function of Reynolds number, and its dependence is given by Beard and Pruppacher (1969) as:

$$\left. \begin{aligned} c_d &= 1 + 0.102 \text{Re}^{-0.55} & 0.2 < \text{Re} < 2 \\ c_d &= 1 + 0.115 \text{Re}^{-0.802} & 2 < \text{Re} < 21 \\ c_d &= 1 + 0.189 \text{Re}^{-0.632} & 21 < \text{Re} < 200 \end{aligned} \right\}. \quad (5)$$

The calculation of droplet trajectories involves considerable computation time, since the equation of motion has to be integrated numerically with respect to time to fully assess the degree to which the droplet deviates from the fluid streamlines. Langmuir and Blodgett (1946) compiled these computations into curves of the collection efficiency  $E$  as a function of two dimensionless parameters, each depending on the free stream velocity, droplet radius and cylinder radius. Collection efficiency is defined as the distance from the centerline of the cylinder axis divided by the cylinder radius that a droplet can be and still be captured by the cylinder, i.e. the far field position of the droplet trajectory that is tangent to the cylinder (Fig. 2). It also refers to that fraction of the total possible droplets in the path of the object that collected. For example, a collection efficiency of 0.5 indicates that half the droplets of a given size would be collected in the cross-sectional area swept out by the cylinder in the flow. Under natural conditions there is usually a variety of droplet sizes, so the computations become lengthy since an equation of motion has to be integrated separately for each size category. The total collection efficiency is then the sum of the collection efficiencies

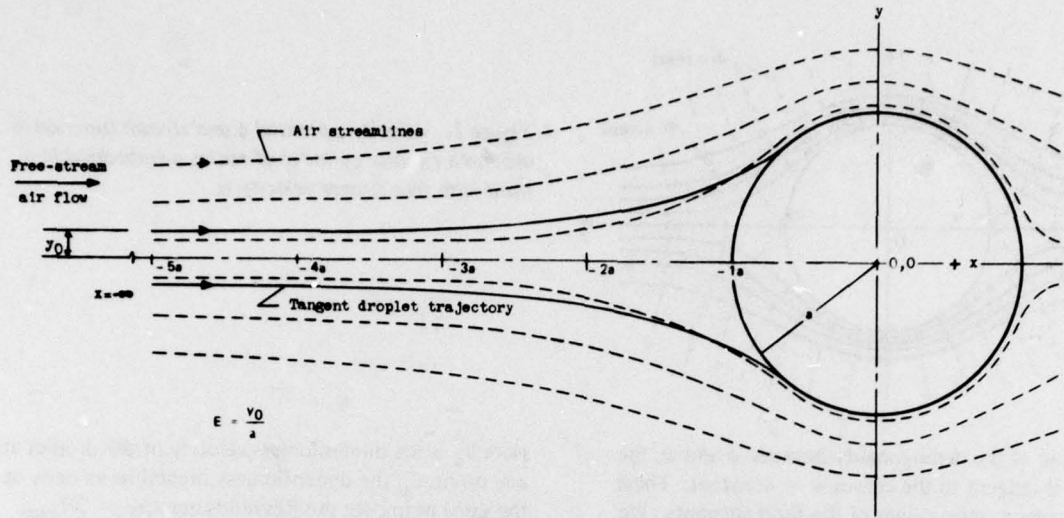


**Figure 2.** Air streamlines and droplet trajectories with respect to a right circular cylinder. Collection efficiency  $E$  is the ratio of the initial far-field  $y$  location  $y_0$  of the droplet trajectory that is just tangent to the radius of the cylinder  $a$ .

for each size times the fraction of the total  $lwc$  represented by that size.

## 2. Time dependence in droplet trajectories

The first of the time-dependent effects that have not been treated in detail in earlier work is that of droplet trajectory. As ice accretes on the front surface of the cylinder it is apparent that the cylinder cannot maintain its initial circular shape. Therefore, the streamline characterized by the boundary of the object is no longer the same as it was initially, and the velocity field in other regions is proportionally distorted to maintain continuity. From eq 5, the change in velocity of the droplet depends on the streamline velocity in that location. The trajectory and velocity of a droplet of a given size will therefore change with time from their values prior to ice accretion, thereby changing the collection efficiency  $E$  as ice accretes. This effect has not been included systematically before because of the length of the computations required to get the initial pre-icing values of the collection efficiency. With a digital computer of sufficient power, however, this effect can be taken into consideration as we show in a later section.

## 3. Thermodynamic processes at the surface of the object

In general, the mass rate of water arriving at the surface of the object (per unit length) can be written as:

$$\dot{m} = E lwc u (2a) \quad \text{kg/m-s} \quad (6)$$

where  $E$  is the collection efficiency, dependent on the velocity, the droplet size, and the object's cross-sectional diameter and characteristic dimensions;  $lwc$  is the volumetric liquid water content ( $\text{kg/m}^3$ );  $u$  is the free stream velocity ( $\text{m/s}$ ); and  $2a$  is the object's cross-sectional diameter normal to the flow ( $\text{m}$ ). However, the mass of ice accreted will not in general be equal to this quantity if heat transfer processes cannot adequately freeze all of the accreted water.

In this formulation it is assumed that 1) radiation terms are excluded since they are small relative to convective and evaporative heat flux, 2) near the object, the droplets have the same velocity as air at that location ( $\approx u_0$ ), 3) the droplets are at thermodynamic equilibrium at temperature  $T_0$ , the ambient air temperature, and 4) the boundary layer thickness is small so the droplet passes through the boundary layer and strikes the surface with the temperature  $T_0$  and velocity  $u$  that it had in the flow. Recent work (List 1977, List et al. 1976, Joe et al. 1976) has indicated some problems with these assumptions, especially with the boundary layer interaction and the droplet's thermal state at high liquid water contents ( $> 0.002 \text{ kg/m}^3$ ). But, as we indicate later, inclusion of different thermodynamics and assumptions can be accommodated in numerical solutions. We employ those just described because of their long usage and their verification, in general terms, by experimental observations.

The heat balance of the surface, controlled by the properties of the flow, is taken as the sum of the

convective and evaporative fluxes, and the aerodynamic heating of the incoming air:

$$Q_{\text{surf}} = -H \left[ (T - T_0) - \frac{R u_0^2}{2c_p \text{air}} + \frac{0.6L_0}{pc_p \text{air}} (E' - E_0) \right]. \quad (7)$$

New terms are  $H$ , the convective heat transfer coefficient (defined below),  $R$ , the surface recovery factor,  $c_p \text{air}$ , the heat capacity of air,  $L_0$ , latent heat of water vaporization,  $E'$ , vapor pressure of water at surface temperature  $T$ ,  $E_0$ , vapor pressure of water at the ambient temperature  $T_0$ , and  $p$ , atmospheric pressure. The factor  $0.6/p$  converts the mass flux from weights of water vapor to the more convenient vapor pressure form, and uses the relationship of latent and sensible heat transfer coefficients of  $H_m/H \approx [F(\text{Le})/c_p \text{air}]$  where  $F(\text{Le})$  [a function of the Lewis number Le (ratio of the diffusion coefficient to thermal diffusivity)] is approximately 1. Therefore,  $H_m \approx (H/c_p \text{air})$ , as indicated in eq 7.

The heat transfer coefficient per unit area,  $H_0$ , is taken from Bosch's formulation (Boelter et al. 1965):

$$H_0 = 31.01 \frac{u^{5.6}}{(2a)^{.44}} \left( \frac{p \cdot 273.16}{1014F^*} \right)^{.56}. \quad (8)$$

Here  $F^*$  is the film temperature  $= (T_0 + T)/2$ . Initially the surface temperature  $T$  is taken as the recovery temperature  $T = T_0 + (R u_0^2/c_p \text{air})$  where  $R u_0^2/c_p \text{air}$  is the aerodynamic heating effect (in  $^{\circ}\text{C}$ ) from compression of the non-icing flow at the stagnation point. The heat transfer coefficient  $H$  is

$$H = H_0 A \quad (9)$$

where  $A$  is the surface area over which the identified processes are taking place, taken as the front half cylinder for our example.

The heat given to the blade by the incoming droplets (mass  $m$  per unit time) is dependent on whether none, some, or all of the water is accreted as ice, that is, the three cases of surface temperature: 1)  $T > 0^{\circ}\text{C}$ , 2)  $T = 0^{\circ}\text{C}$ , 3)  $T < 0^{\circ}\text{C}$ .

#### Case 1. $T > 0^{\circ}\text{C}$

In this case, the heat flux is due to the temperature difference of the collected water plus the conversion of the droplet's kinetic energy into heat:

$$Q_1 = \dot{m} c_p \text{H}_2\text{O} \left( T - T_0 - \frac{u_0^2}{2c_p \text{H}_2\text{O}} \right). \quad (10)$$

#### Case 2. $T = 0^{\circ}\text{C}$

In this case, a fraction  $F$  of the accreted water is converted to ice, adding the latent heat of fusion  $L$  to the heat flux:

$$Q_2 = \dot{m} c_p \text{H}_2\text{O} \left[ (0 - T_0) - \frac{FL}{c_p \text{H}_2\text{O}} - \frac{u_0^2}{2c_p \text{H}_2\text{O}} \right]. \quad (11)$$

#### Case 3. $T < 0^{\circ}\text{C}$

Here all the accreted water is frozen as ice, i.e.  $F = 1$  and the first term in the following equation accounts for the difference in specific heat between the water and ice at temperature  $T$ :

$$Q_3 = \dot{m} c_p \text{H}_2\text{O} \left( T \frac{c_p \text{ice}}{c_p \text{H}_2\text{O}} - T_0 - \frac{L}{c_p \text{H}_2\text{O}} - \frac{u_0^2}{2c_p \text{H}_2\text{O}} \right). \quad (12)$$

The thermodynamic steady-state balance requires that the heat taken by the flow,  $Q_{\text{surf}}$ , is balanced by the appropriate value  $Q_1$ ,  $Q_2$  or  $Q_3$ . In order to choose between these cases, Brun (1957) and Messinger (1953) have taken the heat balance for Case 2 and solved for the frozen fraction  $F$ . If  $F$  is between the limits 0 and 1 then Case 2 is the appropriate one. If  $F > 1$  then Case 3 is applicable, and if  $F < 0$  then Case 1 applies.

In a similar manner, the heat balance as shown schematically in Figure 3 (after Messinger 1953) can be taken for any case, and the residual heat in a short time interval  $\Delta t$

$$Q = (Q_{\text{surf}} - Q_i) \Delta t \quad i = 1, 2, 3 \quad (13)$$

can then be used to modify the surface temperature by

$$T_{\text{new}} = \frac{T c_p \text{m-blade} + Q}{c_p \text{m-blade}}. \quad (14)$$

Here

$$c_p \text{m-blade} = c_p \text{m-blade} + m \cdot F \cdot c_p \text{ice} \quad (15)$$

i.e. the total heat capacity of the object (blade) plus the heat capacity of any accreted ice. The new temperature  $T_{\text{new}}$  can then be checked to see if it is above or below  $0^{\circ}\text{C}$  and the appropriate thermodynamic branch ( $Q_1$ ,  $Q_2$ ,  $Q_3$ ) selected. In going from above or below  $0^{\circ}\text{C}$ , the option  $T = 0^{\circ}\text{C}$  is selected and the appropriate balance chosen based on the value of the accreted fraction  $F$ .  $F$  must lie within the range  $0 < F < 1$  in order for the  $T = 0$  thermodynamics to be chosen.

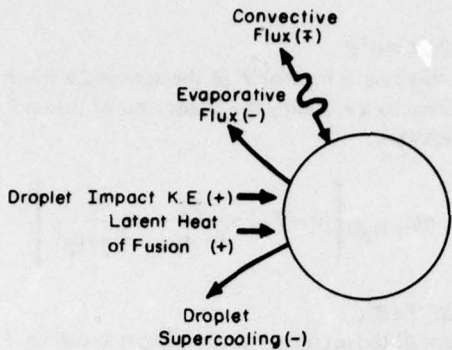


*Figure 3. Schematic indicating the five terms used in the heat balance and whether they are carrying heat toward (+) or away (-) from the freezing surface. Convective flux usually takes heat away from the surface, but at high velocities adiabatic compression of the flow dominates and the convective heat flux is then positive toward the surface.*

#### 4. Time dependence in the thermodynamics

As with the droplet trajectories, the time dependency of the thermodynamics associated with ice accretion basically results from the distortion of the object's size and shape as the ice accretes.

Equation 6 for the mass rate of water collected contains this dependence in the collection efficiency term, which changes as the flow field responds to the increasing accretion. The heat flux from the surface into the flow (eq 7) varies with the change in heat transfer coefficient (eq 9), which in turn varies through the changes in surface area and shape with time. Since the heat fluxes  $Q_i$  additionally depend on the mass rate of water accreted (eq 6), they are also time-dependent in the same manner as the mass rate (i.e. in the collection efficiency  $E$ ). In general, then, the correct form of the equations exhibits significant time dependence. A scheme to update the time-dependent parameters as ice accretion proceeds is described later.

In summary, the major changes in the characteristic manner in which ice accretes on a given object with time are: the variation in the flow field (or collection efficiency) that affects the subsequent mass rate of collection, an increase in surface area that affects the total heat transfer coefficient, and, to a lesser degree, changes in the heat capacity of the object through the addition of ice.

#### 5. Time dependencies of lesser order

##### *Ice density*

The effects described here are less significant but can be quantified to some degree and may be worth-

while including in a detailed description of the icing process. The first of these is the ice density. Macklin (1962) found that in relatively low velocity flows and for surface temperature below 0°C (Case 3 above), the ice density could be obtained as follows:

$$\rho_{ice} = 0.110 \left( \frac{10^4 R_{drop} u_0}{ABS T} \right)^{.76} \text{ (Mg/m}^3\text{). (16)}$$

For ice formed either near the melting point or at higher velocities, or for larger droplets, the density will approach the theoretical maximum density of 0.917 Mg/m<sup>3</sup> and eq 16 will no longer apply. This variation may induce a time dependence since the volume of the ice accretion, as well as its mass, will change the subsequent flow field. The volume can be determined by the mass deposited (eq 6) and the density as given in eq 16.

##### *Run-back icing*

For Case 2 ( $T = 0$ ), only a fraction of the accreted water is initially frozen. In our first formulation we assumed that the unfrozen water is carried away by the flow after imparting its supercooling to the surface and affects neither the thermodynamic processes nor the flow field. Observations during flight tests and on experiments have indicated, however, that icing has occurred on the rear portions of objects as this water flowed back over the surface and refroze. This formation is known as "run-back icing." It is a difficult parameter to include because of the formation conditions—how the water is maintained on the surface and whether heat transfer is rapid enough to freeze it before it is partially or totally removed as liquid at the trailing edge. Cansdale and McNaughton (1977) and Stallabrass and Lozowski (pers. comm.) are currently including a run-back formulation to determine angular dependence of initial icing rate without time-dependence. It appears an extension of the present work with this angular dependent thermodynamics could be a significant step forward in our understanding of the accretion process.

##### *Spongy ice growth*

Spongy ice is formed by a mesh of interlocking dendrites that trap a fraction of the unfrozen water and cause it to freeze by subsequent heat removal, possibly through conduction processes to the side and rear surfaces of the object on which ice is accreting. Spongy ice is not expected to occur frequently under flight conditions because the flow would mechanically disrupt the fragile structure that this ice has when it first begins to form. However, at low velocity (<10 m/s, List 1977) or low Reynolds number, there are indications that spongy ice would exist.

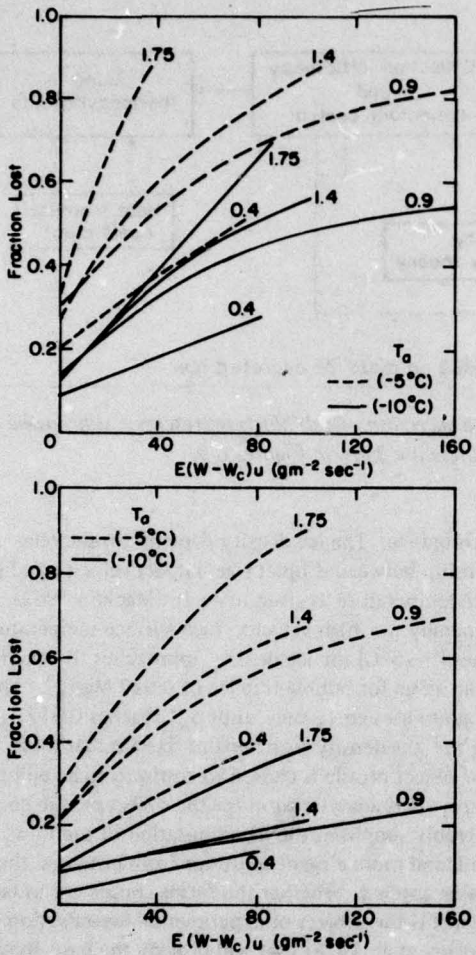


Figure 4. The fraction of accreted water lost plotted against  $E(W - W_c)u$  for various temperatures and average radii (cm) of accreting objects (after Carras and Macklin 1973).

In a previous paper (Ackley 1977) we described how the spongy growth can be incorporated into a full time-dependent solution for icing prediction. Here we briefly describe the variations from the thermodynamics detailed in this report.

The standard thermodynamics are first evaluated to determine that the  $T = 0^\circ\text{C}$  case exists. Instead of a frozen fraction  $F$  depending only on the available heat transfer, empirical relations are used to determine the fraction of the accreted water that is lost to the flow as shown in Figure 4. The quantity  $(W - W_c)u$  is plotted against the fraction lost,  $W$  and  $W_c$  representing the total  $lwc$  and frozen  $lwc$  respectively (i.e.,  $W_c$  corresponds to that amount of  $lwc$  that would raise the surface temperature to  $0^\circ\text{C}$  but still freeze all the

accreted water).  $E(W - W_c)u$  represents the initially unfrozen fraction of the total accreted water, and the curves shown give the fraction lost for various temperatures and radii of the objects. The quantity (1-fraction lost) of initially unfrozen water is that which contributes to the total ice accretion through the spongy ice phenomenon.

In the numerical model, the spongy ice growth could be incorporated by defining a Reynolds number function that determines the changeover from the case where the unfrozen fraction is shed to the case where part of it is incorporated according to the relations shown in Figure 4. Experiments are necessary to verify such a condition since the thermodynamics are dependent upon geometry, the heat capacity of the material, and the characteristics of the flow field in order to freeze additional water over and above that determined for Case 2 ( $T = 0$ ) and may be difficult to quantify.

The shape of the accretion is especially critical since the cross-sectional diameter ( $2a$ ) can be modified by the spongy growth regime, as in the lobe structures seen on hailstones. These changes in shape lead to substantial changes in the subsequent mass rate of accreted water through the collection efficiency effect, the total surface area available for heat transfer, and other first-order feedback effects that are controlled by the cross section.

## NUMERICAL ICE ACCRETION MODEL

### 1. Major subroutines

In a first attempt to include time dependence and its subsequent effects on later ice accretion, a numerical model of the ice accretion processes described has been programmed on a digital computer. The model is programmed in the language Basic on the Dartmouth Time Sharing System (DTSS), which uses a Honeywell 66/40 computer. Hook-up is through an acoustic coupler connected by telephone line to the computer. The model includes software using DTSS subroutines for graphic display of the results using a Tektronix Model 4013 CRT display. A listing of the program, called Ice9, is given in Appendix A. In Figure 5, the feedback effects of time dependence are indicated by the various arrows. The major one is the recomputation of the object's profile after ice accretes, based on the mass of accreted ice and the density variation. The new profile is then used to update the flow field and determines changes, for example in the collection efficiency  $E$  and heat transfer coefficient  $H$ , for the next time step.

Each block of Figure 5 corresponds to a subroutine of the program, and we will describe each of these, keeping in mind their overall interconnection as shown in Figure 5. The initial variables chosen are indicated in Figure 6. These have been described in earlier

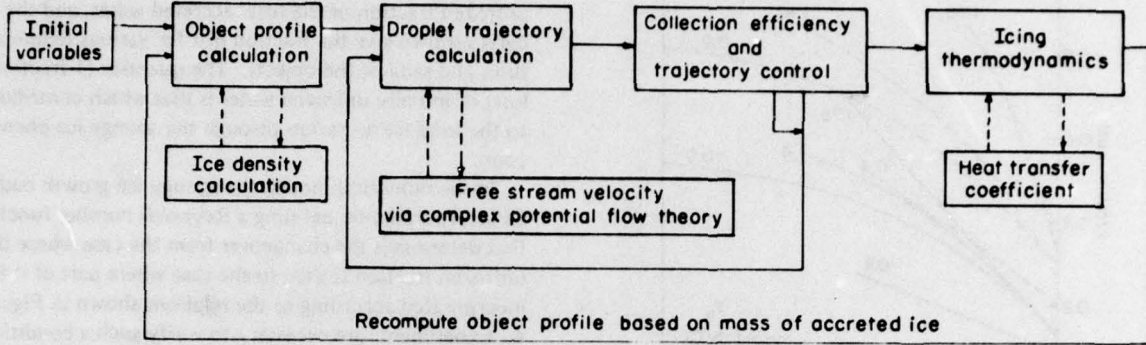


*Figure 5. Block diagram of the numerical model for calculating ice accretion. Each block represents a subroutine of the program. Flow diagrams and pertinent equations for each of these are given in Figures 6-9.*

### Initialize Variables

Air temperature =  $T_0$   
 Liquid water content =  $lw_c$   
 Droplet radius =  $R_D$   
 [or droplet radius distribution =  $P(R_D)$ ]  
 Object airspeed =  $u$   
 [or free stream air velocity]

*Figure 6. Initial variables input in the run control sequence of the numerical model. Other parameters such as the object size and total time of the simulation can also be varied but these require program statement modifications (see Appendix A).*

sections, and we need only mention here that the program is initially set for a circular cylinder of fixed radius and heat capacity, so these parameters are built in as program statements rather than initial variables. They can be varied, however, and comments within the program statements (see Appendix A) indicate the appropriate variables that refer to them. The choice of droplet sizes is controlled by a separate subroutine, Dropdst, which will be described later. The program is initially set to run by asking a series of questions concerning the selection of initial variables, so the choice of either a single droplet size or a number of sizes (e.g. mean and standard deviation for a Gaussian distribution) is automatically routed in the program.

In Figure 7a, the object's profile is recalculated at a time increment set for the given icing conditions. The first step is to take the mass of the icing accretion output by the thermodynamics and the subroutine for ice density (Fig. 7b) and compute the volume of the

accreted ice. The ice density depends on the relationship between droplet size, impact velocity and surface temperature as given in eq 16 (Macklin 1962). Generally, for high velocity, high surface temperature cases ( $> -5^\circ\text{C}$ ) the ice density approaches the maximum value for bubble-free ice of  $0.917 \text{ Mg/m}^3$ . The program uses eq 16 only until  $\rho_{\text{ice}}$  reaches  $0.917 \text{ Mg/m}^3$ ; the density then remains fixed at that value. The new object profile is chosen to conform to an elliptical shape. This analytic form for the object profile considerably simplifies the recomputation of the flow field, and more elegant solutions from potential theory can be applied. Whether the forms chosen are in fact correct is the subject of experimental investigation (Ackley et al. 1978) that will provide the basis for a better estimate of the object profile. At present, the minor axis of the ellipse perpendicular to the flow direction remains constant at the initial value while the major axis parallel to the flow direction is increased in the direction of the accreting ice in relation to the mass and density of the accreted ice (e.g. see Fig. 11, 13, 14). Preliminary experiments indicate that these assumptions are not seriously in error, although observed small changes in cross section can markedly affect the results, since the cross section appears directly in both the mass rate and the thermodynamic equations.

Figure 8 shows the subroutines controlling the computation of the droplet trajectory, the collection efficiency and trajectory control, and the free stream velocity. The subroutine Traject (Fig. 8a) integrates the equation of motion for the droplet, calling upon the subroutine Velocity (Fig. 8c) as needed to determine the velocity of the flow field at each point on the droplet's path, and updates the droplet's position until one of the three cases of interaction with the object is determined. In order to compute the collection

### Object profile calculation [PROFILE]

- 1 Call: subprogram ICE DEN to find density of accreted ice
- 2 The total volume of ice accreted in  $\text{cm}^3$ /(meter of blade/2)

$$V = \frac{m F 1000 \text{ g/kg}}{\rho_{\text{ice}}}$$

- 3 This changes the cross sectional area by

$$V' = \frac{V}{100 \text{ cm}}$$

- 4 New major axis length:

$$a = \frac{4V'}{b^2 \pi} + a$$

a.

### Ice density calculation [ICE DEN]

$$1 \quad \rho_{\text{ice}} (\text{Mg/m}^3) = .110 [10^4 R_{\text{drop}} u_0 / \text{ABS}(T)]^{0.76}$$

(Macklin, 1962)

b.

*Figure 7. Subroutines Profile and Ice Den used to calculate the changes in object profile and ice density from the output of the icing thermodynamics (Thermo, Fig. 9a).*

efficiency for a particular droplet size category, the trajectory that is just tangent to the object must be determined. Therefore, the three cases of the droplet's path are a) where the droplet impacts the object but not at a tangent, b) where the droplet misses the object, and c) where the trajectory is tangent. The interaction status, along with other parameters of this trajectory, is then fed to the Coll Eff subroutine. If the trajectory is not tangent to within an arbitrary amount, this subroutine provides Traject with a new "intelligent" guess for the off-axis starting position of a droplet that will produce a tangent trajectory. Thus Coll Eff serves as the control for Traject, and the program switches between the two subroutines until a tangent interaction is found. Coll Eff then assigns the collection efficiency for the droplet size defined as the starting off-axis (y-value) for the path that ends up tangent to the object, as a fraction of the object's cross section. When

all droplet sizes have been accounted for, basically by the droplet distribution subroutine (Dropdst), the program takes the calculated collection efficiencies and advances into the icing thermodynamics.

Figure 9a shows the subroutine Thermo. This routine takes the output of the collection efficiency routine and the initial variables and computes the mass of ice accreted, based on the thermodynamic balance. The temperature of the object's surface is initialized in the control program at the recovery temperature of a non-icing flow at the same velocity.

The model proceeds through the icing thermodynamics based on the pseudo steady-state temperature hypothesis, i.e. over a small enough increment of time the temperature of the object does not change. So, before the thermodynamic balance is initiated, the heat transfer coefficient is calculated in the subroutine Httrans1 (Fig. 9b), using the current value of the surface

### Droplet trajectory calculation [TRAJECT]

- 1 Calculate  $k$ , (inertial parameter)  $k = \lambda_s/a = 2\rho_w R_{\text{drop}}^2 u / 9\eta a$   
(Langmuir and Blodgett, 1946)
- 2 Calculate Reynolds number of the droplet moving with respect to the air ←
- 3 Calculate the drag coefficient  $c_D$  ( $c_D \text{ Re}/24 = f/6\pi\eta u_d R_{\text{drop}}$ ):  
Beard and Pruppacher (1969) give
 
$$c_D = 1 + 0.102 \text{ Re}^{-0.955} \quad 0.2 < \text{Re} < 2$$

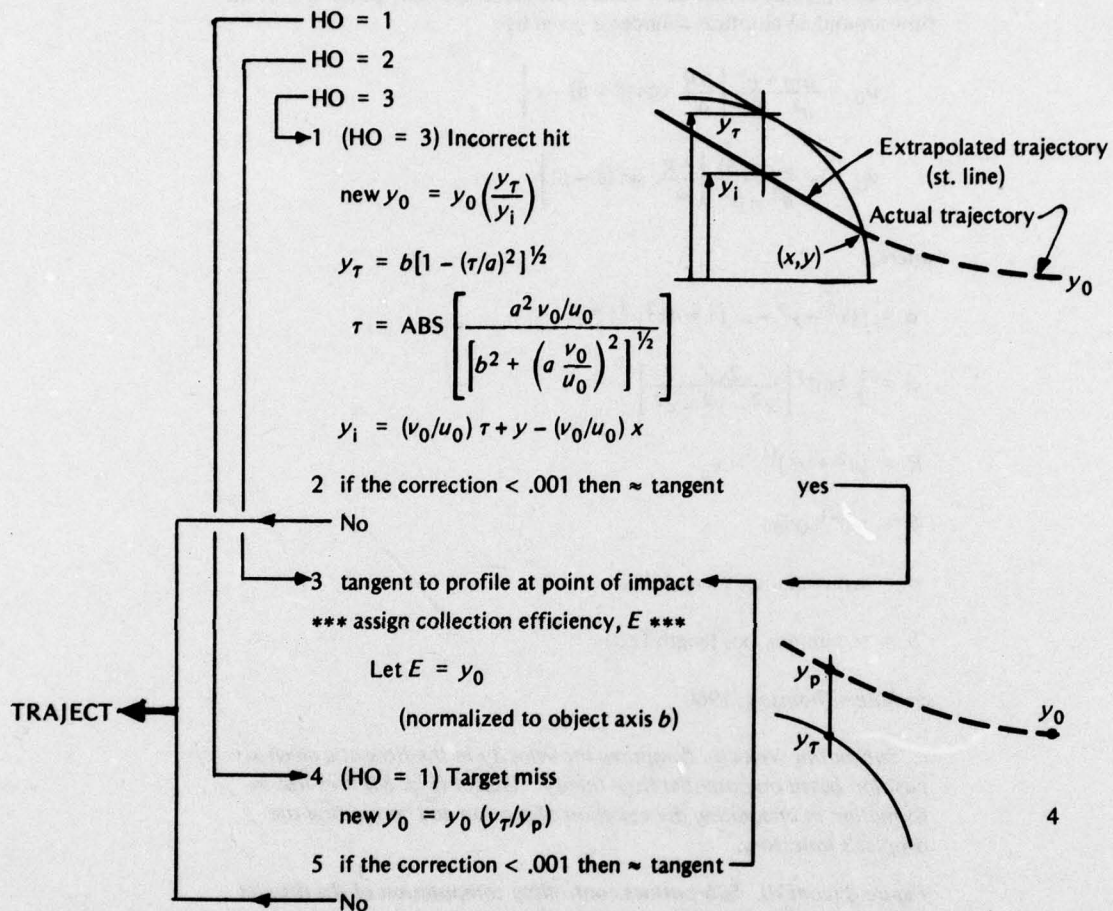
$$c_D = 1 + 0.115 \text{ Re}^{-0.802} \quad 2 < \text{Re} < 21$$

$$c_D = 1 + 0.189 \text{ Re}^{-0.632} \quad 21 < \text{Re} < 200$$
- 4 Call: subprogram VELOCITY for calculating free stream velocity of air  
at droplet's current location
- 5 a)  $du_d = c_D \text{ Re}/24 (u_d - u_0) (dt/k)$  (change in velocity of droplet)
   
b)  $u_d = u_d + du_d$  (new velocity of droplet)
   
c)  $x_d = x_d + u_d dt$  (new position of droplet)
- 6 Is the droplet downstream far enough for it to be capable of hitting the profile, i.e. is
 
$$x_d < a$$
 No      Reiterate →
- 7 Compare the tangent profile and the droplet trajectory tangent ( $v_0/u_0$ )  
if  $|\tan_{\text{profile}}| < |\tan_{\text{trajectory}}|$  No  
yes, then particle (could have) missed profile
- 8 Check to see by how much droplet missed profile
 
$$\text{if } \left( \frac{x^2}{a^2} + \frac{y^2}{b^2} \right) - 1 < .01$$
 then droplet missed profile, but the trajectory was ~ tangent
- 9 \*\* missed profile \*\* let  $H_0 = 1$   
end trajectory
- 10 Did we hit target yet?  $\left( \frac{x}{a} \right)^2 + \left( \frac{y}{b} \right)^2 - 1 < 0$ 
 No      Reiterate →
- 11 Was the trajectory within .1 arctan units of being tangent to the profile
   
No ←
- 12 \*\* tangency found \*\*      Let  $H_0 = 2$ 
  
end trajectory
- 13 Let  $H_0 = 3$ 
  
\*\* incorrect hit \*\*

a. Subroutine Traject uses the object profile output (Fig. 7a) and calls the subroutine Velocity to calculate the free stream velocity (Fig. 8c). It then integrates the equation of motion to determine whether and how a droplet of particular size impacts the object. The HO values are used to indicate the droplet has missed the object ( $HO = 1$ ), hit the object at a tangent ( $HO = 2$ ), or hit the object but not at a tangent ( $HO = 3$ ).

Figure 8. Subroutines controlling computation of the droplet trajectory, collection efficiency and trajectory control, and free stream velocity.

**Collection efficiency calculation and trajectory control**  
**[COLL EFF]**



b. Subroutine Coll Eff takes the droplet trajectory information to compute the collection efficiency  $E$  for the given droplet size and object profile. If the correct tangency value of droplet impact is not found, the subroutine readjusts the droplet's initial off-axis position ( $y_0$ ) and calls Traject to compute the correct tangent trajectory. Once the collection efficiency is assigned, the program proceeds to Thermo (Fig. 9a).

Figure 8 (cont'd).

temperature. Then, based on the current surface temperature, the appropriate thermodynamic expression is chosen (Fig. 9a). The complete thermodynamic balance yields the new surface temperature, or new ice fraction accreted if in the  $T = 0^\circ\text{C}$  temperature regime. Of course, care must be taken to maintain physical as well as thermodynamic continuity as the temperature proceeds through the limits of each thermodynamic argument. The program checks for errors in continuity and redirects execution at the appropriate level.

At the end of the icing thermodynamics, the output

is given as new ice mass, total heat capacity, and surface temperature. After several iterations of the thermodynamics, the new total ice mass is fed back to the object profile calculation (Fig. 5, 7) to recompute the object's size, flow field characteristics, and surface area for the next time period of the calculation.

#### 2. Options for droplet size variations

In addition to the basic computational portions just discussed, the Dropdst subroutine allows the specification of more than one droplet size for any given simulation. Dropdst has three options available on

### Stream velocity [VELOCITY]

From complex potential flow theory the velocity at any point  $x, y$  in the flow around an elliptical cylinder is given by:

$$z_0 = \frac{u(a+b)}{a^2 - b^2} \left[ \frac{bR}{\alpha} \cos(\theta - \beta) - a \right]$$

$$v_0 = -\frac{u(a+b)}{a^2 - b^2} \left[ \frac{bR}{\alpha} \sin(\theta - \beta) \right]$$

where:

$$\alpha = [(x^2 - y^2 - c^2)^2 + 4x^2y^2]^{1/4}$$

$$\beta = \frac{1}{2} \tan^{-1} \left[ \frac{2xy}{x^2 - y^2 - c^2} \right]$$

$$R = (x^2 + y^2)^{1/2} = x_d$$

$$\theta = \tan^{-1}(y/x)$$

$$a = \text{semimajor axis length } (\parallel u)$$

$$b = \text{semiminor axis length } (\perp u)$$

see Milne-Thomson, 1960

c. Subroutine Velocity computes the velocity in the flow at a given  $x, y$  position based on potential flow theory. Traject (Fig. 8a) uses this information in integrating the equation of motion and computing the droplet's trajectory.

*Figure 8 (cont'd). Subroutines controlling computation of the droplet trajectory, collection efficiency and trajectory control, and free stream velocity.*

droplet distributions in addition to the single droplet size, which does not require the calling of the Dropdst subroutine. Currently the droplet distributions available are a Gaussian, an Erlang of order 1, 2 or 3, or a histogram of sizes that could be, for example, from experimental data. In running the program, the operator is asked to specify whether a distribution is desired and, if so, this subroutine is called. It then asks additional questions concerning the type of distribution desired and the necessary parameters for specification of this distribution.

#### Gaussian distribution

The program asks for the mean, radius variance and total number of droplet sizes desired up to a maximum

of nine sizes. The subroutine then apportions the available liquid water content (specified initially in the control sequence) into these categories in such a way that the total number of droplets conforms to the distribution as specified. The Gaussian is sampled between  $\pm 2$  standard deviations of the mean so that it includes 95% of the distribution.

#### Erlang distribution

The Erlang distribution is of the form

$$F_r(r - r_0) = \frac{\lambda^k (r - r_0)^{k-1} e^{-\lambda(r-r_0)}}{(k-1)!} \quad (17)$$

## Icing thermodynamics [THERMO]

- 1 Calculate the ambient water vapor pressure ( $E_0$ )  
*Smithsonian Meteorological Tables, 1951*
- 2 Call: subprogram HTTRANS1 for calculating heat transfer coefficient  
[watts/ $^{\circ}\text{C}$  (meter of blade/2) sec]
- 3 Calculate mass of water collected/meter of blade · sec

$$m = E \cdot lwc \cdot u \cdot b$$

- 4  $T < 0$
  - $T = 0$
  - $T > 0$
- branch to appropriate thermodynamics  
(see E.A. Brun, 1957)

initially,  

$$T = T_0 + \frac{u_0^2}{2000}$$
  
i.e. recovery temp

5  $T > 0$  what is Q?

a) 
$$Q = -H \left[ T - T_0 - \frac{R u_0^2}{2c_{p\text{air}}} + .6 L_0 (E' - E_0) / p c_{p\text{air}} \right] -$$
  

$$-m c_{p\text{H}_2\text{O}} \left( T - T_0 - \frac{u_0^2}{2c_{p\text{H}_2\text{O}}} \right)$$

$R$  = surface recovery factor

$L_0$  = latent heat of vaporization of water @  $0^{\circ}\text{C}$

$E'$  = vapor pressure of water at surface temperature

b) Calculate new  $T$

$$T = (T c_{p\text{mblade}} + Q) / c_{p\text{mblade}}$$

c) Is  $T$  still above  $0^{\circ}\text{C}$ ?

\*\* end THERMO \*\*

No

6  $T = 0$

a) 
$$Q = -H \left[ -T_0 - \frac{R u_0^2}{2c_{p\text{air}}} + .6 L_0 (E' - E_0) / p c_{p\text{air}} \right] -$$
  

$$-m c_{p\text{H}_2\text{O}} \left( -T_0 - \frac{F L}{c_{p\text{H}_2\text{O}}} - \frac{u_0^2}{2c_{p\text{H}_2\text{O}}} \right)$$

$F$  = fraction of collected water accreted as ice

$L$  = latent heat of freezing

b)  $F = F - Q/Lm$

c) is  $F > 0$

Temperature above  $0^{\circ}\text{C}$

No

d) is  $F < 1$

Temperature goes below  $0^{\circ}\text{C}$

No

e)  $c_{p\text{mblade}} = c_{p\text{mblade}} + m F c_{p\text{ice}}$

\*\* end THERMO \*\*

7  $T < 0$

a) 
$$Q = -H \left[ T - T_0 - \frac{R u_0^2}{2c_{p\text{air}}} + .6 L_0 (E' - E_0) / p c_{p\text{air}} \right] -$$
  

$$-m c_{p\text{H}_2\text{O}} \left( T \frac{c_{p\text{ice}}}{c_{p\text{H}_2\text{O}}} - T_0 - \frac{L}{c_{p\text{H}_2\text{O}}} - \frac{u_0^2}{2c_{p\text{H}_2\text{O}}} \right)$$

b)  $T = (T c_{p\text{mblade}} + Q) / c_{p\text{mblade}}$

c)  $c_{p\text{mblade}} = c_{p\text{mblade}} + m c_{p\text{ice}}$

SUBEND

a. Subroutine Thermo calculates mass of water arriving and converted into ice or shed as unfrozen water if  $T > 0^{\circ}\text{C}$ .

Figure 9. Based on the ambient conditions, the calculation of mass accreted is completed by incorporating the thermodynamics at the surface.

**Heat transfer coefficient**  
[HTTRANS1]

$$1 \quad H_0 = 31.01 u_0^{0.56} / (2a)^{.44} \left( \frac{\rho * 273.16}{1014 F^*} \right)^{.56} \quad \frac{\text{watts}}{\text{m}^2 \text{ } ^\circ\text{C sec}}$$

$$F^* = \text{film temperature} = \frac{T_0 + T}{2}$$

$$2 \quad \text{the total heat transfer coefficient} \quad \frac{\text{meter of blade}}{2}$$

$$H = H_0 \pi \frac{a+b}{4} \left( \frac{1}{100} \right)$$

b. Subroutine Httrans1 computes the total heat transfer coefficient based on the current surface temperature and object dimensions. It is called by Thermo (Fig. 9a) as needed.

Figure 9 (cont'd). Based on the ambient conditions, the calculation of mass accreted is completed by incorporating the thermodynamics at the surface.

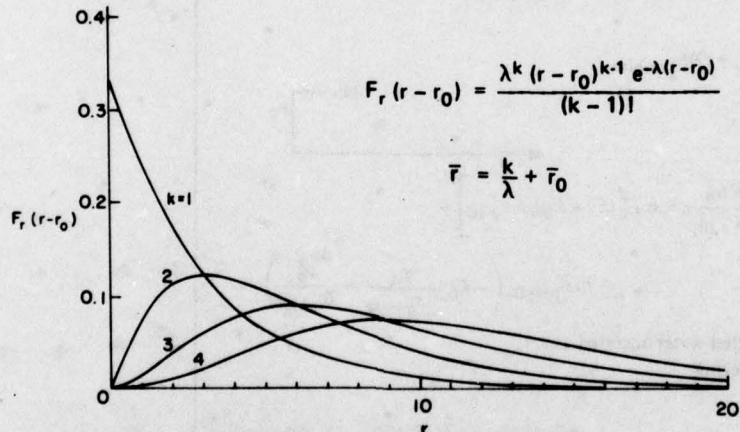


Figure 10. Forms of the Erlang distribution for various values of the parameter  $k$  as shown. The "start radius"  $r_0$  is zero for these cases.

and has the forms shown in Figure 10 for various values of the "Erlang order"  $k$  and for "start" values  $r_0 = 0$ . The mean or expected value of the distribution is

$$\bar{r} = \frac{k}{\lambda} + r_0. \quad (18)$$

As Figure 10 shows, a variety of distributions can be obtained by specification of a few parameters

$(k, \lambda, r_0)$ , making it easy to change the characteristics of the distribution for simulation comparisons. The distributions are also more reminiscent of the variety one sees in real cloud droplet distributions than the Gaussian distribution (Mason 1971). The subroutine asks the specification of the values of  $k, \bar{r}, r_0$  and the number of droplet classes, up to a maximum of nine, that are desired. The subroutine then calculates the value of  $\lambda$  from eq 18 and apportions the available  $w/c$  into the specified classes according to eq 17. The

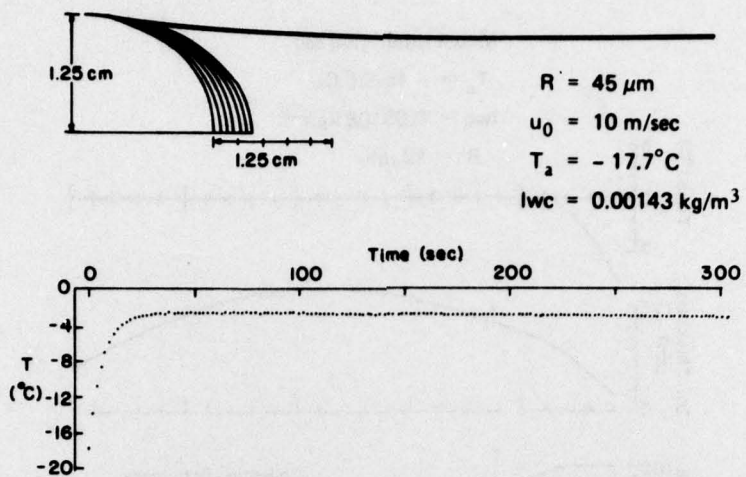


*Figure 11. (Top) The change in profile dimension at 50-s intervals by ice accretion is indicated by the profile shapes on the initial half cylinder. The black line coming from the right is the tangent trajectory at the beginning (top of the black line) and end (bottom of the black line) of the icing period of 300 s. (Bottom) The surface temperature of the front half cylinder as a function of time is plotted. As seen, the surface temperature reaches an equilibrium value within about 30 s after the icing starts.*

subroutine samples the distribution from the start radius  $r_0$  to the value  $r_0 + 2 \times \bar{r}$ .

#### *Histogram distribution*

Dropdst also allows the specification of an arbitrary distribution such as may be obtained during experiments or in airborne sampling. In this case, the input to the subroutine is the number of droplet sizes (up to nine) and pairs of values that indicate the droplet radius and its percentage contributions to the total numbers. The subroutine then computes the volume percentages and the total number required to equal the designated  $IWC$ .

#### **3. Option for the helicopter rotor case**

As mentioned in the introduction, helicopters have serious icing problems since they normally operate at the altitudes where icing conditions most often occur. They also have the interesting characteristic that the linear velocity of the rotating blade varies over a large range (eq 1), from essentially near zero in the hub region to nearly sonic at the blade tip. Interest in how these changing conditions influence ice accretion processes was a continuing impetus in the development of this numerical scheme. Two options to include the velocity variability were therefore built into the program.

The first of these selects specific values of the velocities and computes the ice mass and profile changes

as a function of time. Figure 11 shows such a calculation for a velocity of 10 m/s and initial conditions of  $0.00143 \text{ kg/m}^3 / IWC$ , droplet radius of  $45 \mu\text{m}$  and  $T_a = -17.7^\circ\text{C}$ . Any number of these velocities can be selected, allowing details of the ice accretion process to be seen, such as the time dependence of the collection efficiency or heat transfer. The heavy black line is the tangent trajectory used to compute the collection efficiency for this case. Examples of these will be shown in the next section. The figure illustrates the three main time intervals of the calculation. The spacing of the dots in the temperature plot indicates the time period (2 s) that we take for the pseudo steady-state heat balance, i.e. in the 2-s time interval the thermodynamic properties of the system do not change. After 25 repetitions of the thermodynamic balance with successive updates of the heat flux, the profile dimensions are sufficiently changed to require the updating of the collection efficiency, ice mass and profile shape characteristics. These updates take place at 50-s intervals, as indicated by the marks on the time scale. The changes in the profile dimensions indicated on the figure take place at these intervals. The third interval is the total time of the calculation, indicated by the full-scale length of the time scale (300 s). Programming mechanics dictate that these times be integer multiples of the smallest value. However, they can be modified within this constraint.

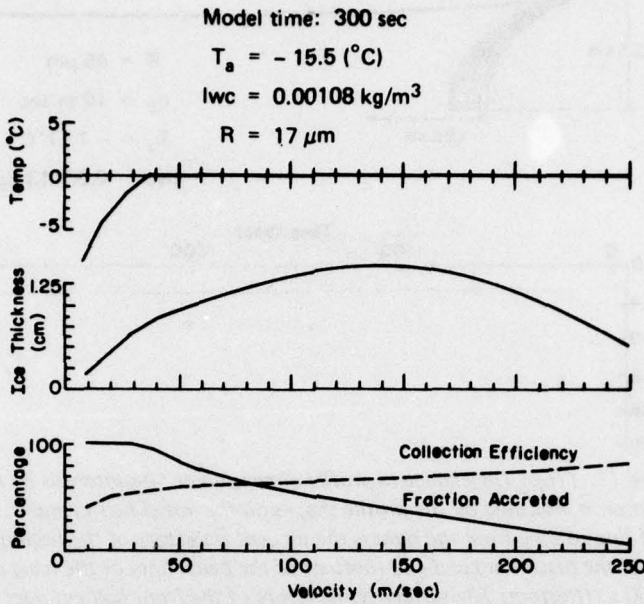


Figure 12. Numerical simulation of helicopter rotor blade icing showing the surface temperature, leading edge ice thickness, collection efficiency and fraction accreted (as ice) as a function of velocity for the initial conditions as shown. The maximum ice thickness occurs when heat transfer conditions optimize with amount of accreted water (eq 6) to form the most ice.

The second display option is shown in Figure 12. Here the three quantities equilibrium surface temperature, leading edge (maximum) ice thickness, and variations of collection efficiency and fraction of collected water accreted as ice are given as a function of velocity along the blade from 0 m/s to 250 m/s. The program computes and stores the heat balance, ice thickness, and collection efficiency for each 10-m/s velocity interval for a period of 300 s and then steps to the next velocity value. When this has been accomplished for 25 velocity values (0 to 250 m/s in 10-m/s intervals), the information saved at the end of each calculational step is displayed. Straight lines are drawn between the points to complete the curves as shown. In addition, the lowest plot shows the percentage of the accreted water that is frozen into ice. As shown for this particular plot, the fraction accreted and frozen drops below 100% at the point where the surface temperature rises to 0°C as the thermodynamic equations would indicate.

As shown in Figures 11 and 12 the program also includes software for plotting data. These are given by the subroutines Plot T, Pt Blade, Plot D, Plot M and Thermost. The function of each of these is described in the comments accompanying the program

listing in Appendix A. In addition to the plots shown in Figures 11 and 12, the program can also show a plot of the droplet size distribution if a distribution is selected. The variation of the thermodynamic quantities given in eq 7, 10, 11 and 12 as a function of segment velocity (similar to the surface temperature plot in Figure 12) can also be plotted. The quantities plotted are the convective flux, evaporative flux, kinetic energy of impact term, the latent heat requirement to freeze the accreted water, and the influx term of heat (negative) due to droplet supercooling. These are defined in eq 7, 10, 11 and 12 and discussed more fully in the following section.

## RESULTS

In this section, we give some examples of the effect of including the time dependence as formulated previously. First, the effects of including collection efficiency feedback and a distribution of droplet sizes are shown in Figure 13.

Here the amount of ice accreted as time proceeds is plotted for the initial conditions of  $lwc = 0.00108 \text{ kg/m}^3$ , initial ambient air temperature =  $-5.5^{\circ}\text{C}$ , and

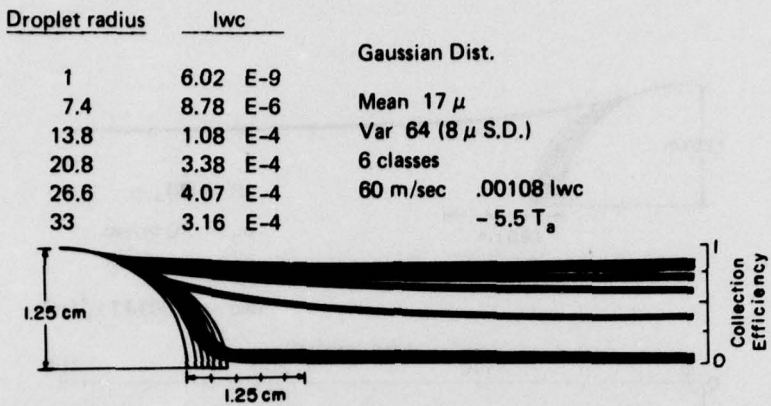


Figure 13. Droplet trajectories and ice profile changes for a Gaussian droplet size distribution. Droplet sizes and respective liquid water contents are given in the inset; the collection efficiencies for the various droplet categories and their changes with profile dimension changes are given on the right hand scale. Profile ice thickness changes are shown at 50-s intervals. Thermodynamic conditions for this simulation are such that the surface temperature was at  $0^\circ\text{C}$  (equilibrium) and some accreted water was not frozen.

velocity = 60 m/s. The droplet distribution selected is a Gaussian with six classes. The mean radius is  $17\mu$  ( $17 \times 10^{-6} \text{ m}$ ) and the droplet radius standard deviation is  $8\mu$  about the mean. As shown by the inset table listing the IWC amounts by droplet size, very little of the total water available is partitioned into the lower droplet sizes (for the two lowest droplet sizes the IWC is 2 to 3 orders of magnitude lower than for any of the four higher classes).

Referring to the profile plots, the dark lines originating at the right refer to the collection efficiency and its changes with time and droplet size as shown. The thickness of these lines results from "overprinting" on the display screen so the top of the line for any droplet class is the tangent trajectory that, when scaled to the object radius, gives the initial value of collection efficiency for that class (scale at right). The bottom of each thick line is the final collection efficiency value after 300 s of ice accretion has taken place. For the largest droplets ( $> 20.2\mu$ ) the collection efficiencies are generally 0.75 or above for this velocity. The collection efficiency drops markedly for sizes below  $20\mu$  and the decrease in collection efficiency with ice accretion (given by the distance between the top and bottom trajectories or thickness of each line) is also greater for the smaller droplets. The ice accretion rate, shown by the changes in the object's profile at 50-s intervals, does not change dramatically since 90% of the liquid water is concentrated in the three largest droplet classes. The collection efficiencies for these classes vary by the smallest amounts (~ 3 to 5%) at this velocity and

object radius, so the rate of ice thickness change is not substantial for the time period of this simulation. It is easily seen from this plot, however, that a lowering of the mean droplet size such that a significant shift occurs in the amount of IWC available in small droplets ( $< 14\mu$  radius) would substantially change the ice accretion rate. The collection efficiency and its change with object profile are both more markedly affected at the lower droplet sizes; for example the collection efficiency of the  $1\mu$  category changes from 15% to 6%, a 60% change with the object profile change.

We illustrate this further in Figure 14 where two profiles are shown for the same conditions except that the droplet size is given as  $30\mu$  on the top, and half that,  $15\mu$ , on the bottom. From this figure we see that the total center line ice thickness is reduced by 40% by changing the droplet radius, even though the ambient temperature and liquid water content are the same for both cases. Similarly, the calculated surface temperature is higher for the larger droplets since more latent heat is liberated per unit time, which increases the heat flux to the object surface and increases its temperature.

A more complete treatment of the comparison between experimental results and model simulations will be the subject of later reports. These comparisons are important because of their use in updating model results and improving on portions such as the object profile shape and heat transfer coefficient which are currently based on assumptions (e.g. the time period of steady-state thermodynamics) that may require modification. In Figure 15, we compare and discuss one such simulation with experimental data to

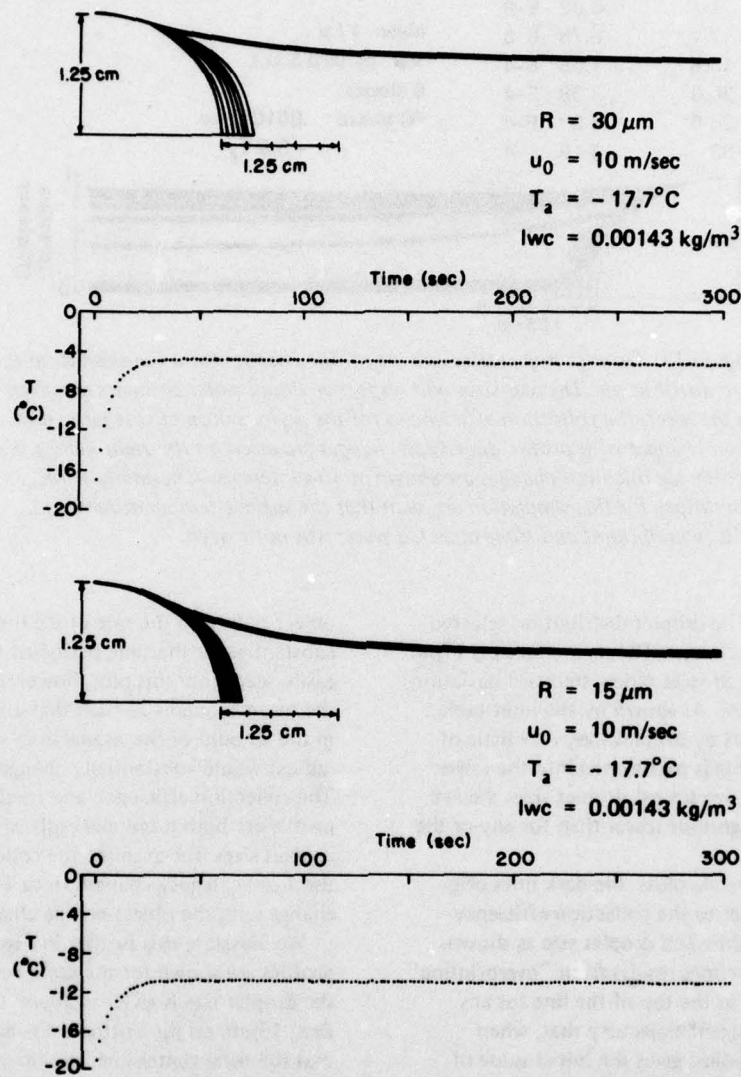


*Figure 14. Accreted ice thickness and temperature for the ambient conditions indicated. The profile updates occur at 50-s intervals. The difference in accreted ice thickness for the two cases occurs because of the change in collection efficiency for the droplet sizes 30  $\mu\text{m}$  (top) and 15  $\mu\text{m}$  (bottom).*

indicate both the general validity of the model and some specific differences that require more experimentation and better model parameterization. This figure, in the ice thickness distribution portion, shows the simulated and experimental results. This experimental result has been previously discussed in Ackley (1977) and is more fully described there. Briefly, the measurements were taken from a rotating cylinder

system at 3600 rpm in a coldroom at the ambient temperature shown. Water of the mean droplet size and lwc indicated was sprayed onto the rotor. Comparing the two ice thickness curves it is seen that the simulated ice thickness is somewhat less than the experimental accumulation but is reasonable within the constraints imposed by both the assumptions in the simulation (e.g. one droplet size at the mean

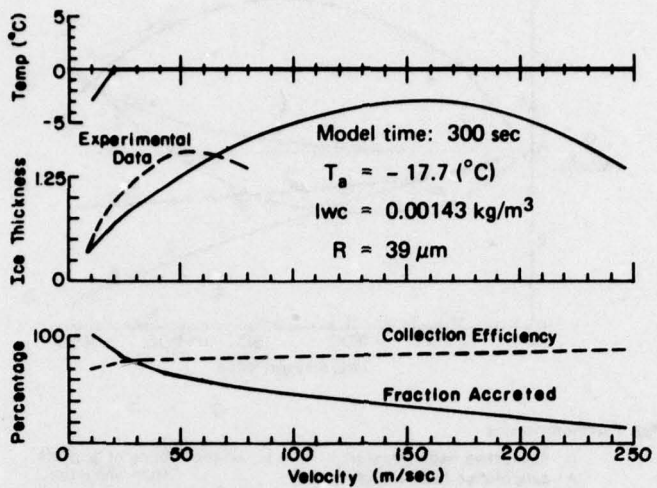


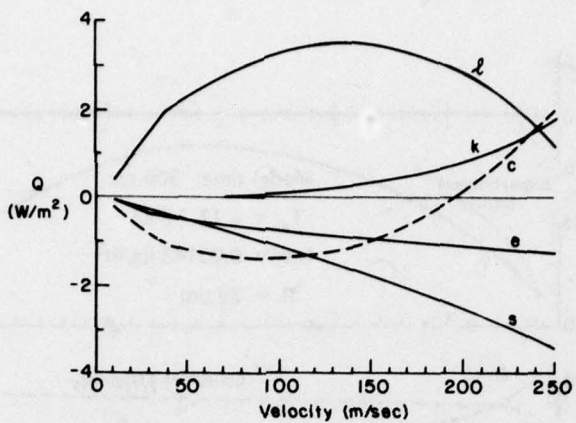
*Figure 15. Comparison between experimental data (ambient conditions inset) and model simulation of the same conditions. Agreement is reasonable considering experimental errors in lwc (~ 25%) and use of a single droplet size (mean experimental size) in the simulation compared to a distribution in the experiment.*

experimental value) and the errors in measurement in the experiment on both droplet size and lwc (~ 25%). In the experiment, analysis of the ice properties showed a grain size change, indicating a transition in surface temperature from  $T < 0^\circ\text{C}$  to  $T = 0^\circ\text{C}$  in the vicinity of the blade where the linear velocity was 20 m/s. As shown by the calculated temperature distribution (top of Fig. 15) the calculated rise to  $0^\circ\text{C}$  takes place in about the same velocity region. This agreement would indicate the simulated heat transfer and thermodynamic relations are approximately compatible with the experimental measurements.

The location of the maximum ice thickness in the experimental data differs from that in the simulation. The latter indicates that the ice thickness should be increasing all the way to the tip of the experimental rotor ( $v \sim 100$  m/s) for this set of conditions. However, a set of experiments in which the lwc and droplet distributions were held constant while the ambient temperature was varied showed that the location of the experimental maximum ice thickness varied only slightly with ambient temperature at roughly the same location shown in Figure 15. This continuity between the experiments indicates the maximum position may be controlled by, for example, a flow field perturbation induced by the blunt end of the cylindrical rotor. We plan further experiments at different rotation rates (i.e. changing the velocity distribution without changing the physical dimensions of the rotor) to see if and how

this effect is modified. At this time, therefore, the difference in the position of the thickness maximum between the experiments and the simulation cannot be resolved until further experimental results are available that can test the end effects of the rotor tip.

In Figure 12 we showed the accumulated ice for the conditions as indicated. Figure 16 gives the relative contributions of the thermodynamic terms for the same conditions, which we now discuss more fully. The heat balance requires that the algebraic sum of the positive and negative contributions to the heat flux equal zero as long as ice is accreting (Fig. 16). If the balance goes positive, then the excess heat is accounted for by a rise in surface temperature (eq 14). At velocities below 50 m/s, Figure 16 shows that the convective flux dominates, contributing about 50% of the necessary heat flux to freeze the accreted water, with smaller and nearly equal contributions from droplet supercooling and evaporative heat flux of approximately 25% each. At about 80 m/s, the convective flux is at its maximum negative value; it then becomes less negative with increasing velocity because of the contribution to this flux by adiabatic compressional heating of the flow ( $Ru^2/2c_p$  term in eq 7). Above 80 m/s, an additional positive term, the kinetic energy imparted by droplet impact, also becomes significant. The increasing positive contribution of these terms causes the amount of heat to balance



**Ice Thermodynamics**

- |  |  |
|--|--|
| c convective heat transfer                   | k kinetic heating of droplets from impact          |
| e evaporative heat transfer                  | f latent heat requirement to freeze accreted water |
| s influx of $q$ due to droplet super-cooling |  |

*Figure 16. Magnitude of the individual thermodynamic terms as a function of velocity for the simulation shown in Figure 12. The terms are defined in Figure 9a and by eq 7, 10, 11 and 12.*

the latent heat of freezing to peak and then drop off since the other negative terms, the evaporative and supercooling influx, decrease more slowly with velocity than the positive terms are increasing. The maximum available latent heat requirement corresponds to the maximum ice thickness at 140 m/s since we are in the 0°C surface temperature region (Fig. 12, top). At the maximum ice thickness, the heat necessary to freeze the accreted ice is about 45% from droplet supercooling, 25% from evaporative flux and 30% from convective flux. Kinetic energy of the droplets consumes about 7% of the heat at this point, the remainder being balanced by the latent heat of freezing. No heat is available for freezing from convective flux above 200 m/s due to the heating effects of adiabatic compression. At about 240 m/s, the kinetic energy of droplet impact, the now positive convective flux, and the latent heat of freezing all consume equal amounts of the negative flux available from evaporative flux and droplet supercooling.

#### CONCLUSIONS AND FUTURE STUDIES

As pointed out earlier, one important result of the numerical model is that a more accurate comparison of theory with experimental results is made possible by including time dependence in a measurable way.

These comparisons can provide more confidence in the simulation of conditions that are not experimentally known. For example, it is clear from Figures 13 and 14 that a change in either mean droplet size or in the distribution such that large numbers of small droplets compose much of the liquid water content can radically change the amount of ice accreted. Using ground icing sprayers with large droplet sizes for tests representing cloud conditions may therefore be highly inaccurate. As mass accretes the collection efficiency changes with time and is also a function of droplet size. The numerical solution graphically portrays (Fig. 13, 14) how these conditions can affect the ice buildup for a given set of initial conditions.

In a situation such as icing of a helicopter rotor blade, the thermodynamics determining the ice buildup at any particular linear velocity can show wide variability as to which terms dominate, so a numerical solution and graphic display can provide a convenient method of seeing this variability (Fig. 12, 16). For design purposes, additional terms, for example, increasing the heat flux to the blade surface by electrical heating, can be evaluated to determine whether particular icing conditions would be relieved or unaffected by the extra heat flux. An optimization procedure could then be used with statistics on meteorological conditions to evaluate the likelihood of the design change significantly increasing the chances for successful operation.

Future changes in the model will include a continuing comparison with experimental data to determine more exactly the physics controlling the icing process. Evidence exists that cross section and object shape can change considerably with changing meteorological conditions, especially at higher temperature (Dickey 1952), so a change in the way these parameters are included is probably necessary. Preliminary comparisons with experiments at temperatures below  $-25^{\circ}\text{C}$  (Ackley et al. 1978) indicate that the observed total ice thickness after a few minutes of accretion is less than what is predicted in the current simulation. This difference may result from a more rapid lowering of collection efficiency with ice accretion than that currently used, necessitating a reevaluation of the flow field taking into account that the object shape is irregular and not elliptical. List (1977) has also indicated that use of potential flow should be modified to include significant boundary layer effects near the object. These are not now in the model, but can be parameterized as long as experimental evidence indicates they are necessary. Finally, the most difficult parameterization involves the thermodynamics since it is the most complex and relies on the most assumptions. A major reliance is on an assumed heat transfer coefficient based on our best present knowledge. This coefficient is then used to derive the highly important surface temperature. Experiments using isotopic analysis (deuterium: hydrogen and oxygen-18:oxygen-16 ratios) on the accreted ice can perhaps be used to derive the surface temperature and independently verify our choice of heat transfer coefficient. The importance of heat flow through the back surface of the object and the variation of the heat transfer with time and conditions may then be better parameterized for model prediction use.

At present, within the data limitations that have been used for its formulation, the model offers a significant method of evaluating time dependence (or independence) of the various parameters that influence the icing process. With this information, extension to engineering design may be facilitated by easy access to a number of simulated "case histories" applying to aircraft icing or ground-based structural problems. Total icing loads can be computed by breaking the structure down geometrically, treating each shape individually, and summing up the individual loads into the total for the structure.

The beauty of the model lies in its subroutine construction, which allows updating of particular aspects (flow field, thermodynamics) as more evidence becomes available, without the need for completely altering those portions that are substantially proven.

The utility of including a more complex formulation can then be easily checked against how it changed the net result. In the present formulation, we have determined, for example, that the inclusion of a complete droplet distribution function compared to using the mean droplet size does not significantly affect the total mass accreted for most problems of engineering interest where droplet sizes exceed about  $20\text{-}30\mu\text{m}$  in radius.

## LITERATURE CITED

- Ackley, S.F. (1977) A numerical ice-accretion model. *Journal of Glaciology*, vol. 19, p. 665-6. (Abstract of paper presented at Applied Glaciology Symposium.)
- Ackley, S.F., G. Lemieux, K. Itagaki and J. O'Keefe (1978) Laboratory experiments: The icing of rotating blades. TRB Symposium on Snow and Ice Control Research, Hanover, May, 1978.
- Beard, K.V. and H.R. Pruppacher (1969) A determination of the terminal velocity and drag of small water drops by means of a wind tunnel. *Journal of Atmospheric Science*, vol. 26, no. 5, p. 1066-72.
- Boelter, L.M.K., V.H. Cherry, H.A. Johnson and R.C. Martinelli (1965) *Heat transfer notes*. N.Y.: McGraw-Hill, p. 506-8.
- Brun, E.A. (1957) Icing problems and recommended solutions. AGARDograph 16, NATO, 69 p.
- Cansdale, J.T. and I.I. McNaughton (1977) Calculation of surface temperature and ice accretion rate in a mixed water droplet ice crystal cloud. Royal Aircraft Establishment Technical Report 77090, Farnborough, Hants, U.K.
- Carras, J.N. and W.C. Macklin (1973) The shedding of accreted water during hailstone growth. *Quarterly Journal of the Royal Meteorological Society*, vol. 99, p. 639-48.
- Dickey, T.A. (1952) An analysis of the effects of certain variables in determining the form of an ice accretion. U.S. Navy, Naval Air Material Center, AEL-1206.
- Joe, P.I. et al. (12 others) (1976) Loss of accreted water from growing hailstones. In preprints, International Conference on Cloud Physics, July 26-30, 1976, Boulder, Colorado, American Meteorological Society, p. 264-69.
- Knight, C.A. and N.C. Knight (1968) The final freezing of spongy ice: Hailstone collection techniques and interpretation of structures. *Journal of Applied Meteorology*, vol. 7, no. 5, p. 875-881.
- Langmuir, I. and K.B. Blodgett (1946) Mathematical investigations of water droplet trajectories. G.E. Report RL-244. Reprinted in *Collected Works of I. Langmuir*, Pergamon Press, p. 335-393.
- List, R., J.G. Cantin and M.G. Ferland (1971) Structural properties of two hailstone samples. *Journal of the Atmospheric Sciences*, vol. 27, p. 1080.
- List, R. et al. (12 others) (1976) On the variation of the collection efficiencies of icing cylinders. In preprints, International Conference on Cloud Physics, July 26-30, 1976, Boulder, Colorado, American Meteorological Society, p. 233-39.
- List, R. (1977) Ice accretion on structures. *Journal of Glaciology*, vol. 19, no. 81, p. 451-66.

- Macklin, W.C. (1962) The density and structure of ice formed by accretion. *Quarterly Journal of the Royal Meteorological Society*, vol. 88, p. 30-50.
- Macklin, W.C., J.N. Carras and P.J. Rye (1976) The interpretation of the crystalline and air bubble structures of hailstones. *Quarterly Journal of the Royal Meteorological Society*, vol. 102, p. 25-44.
- Macklin, W.C., C.A. Knight, H.E. Moore, N.C. Knight, W.H. Pollock, J.N. Carras and S. Thwaites (1977) Isotopic crystal and air bubble structures of hailstones. *Journal of Atmospheric Science*, vol. 34, p. 961-967.
- Mason, B.J. (1971) *The physics of clouds*. Oxford: Clarendon Press, 2nd Edition.
- Messinger, B.L. (1953) Equilibrium temperature of an unheated icing surface as a function of airspeed. *Journal of Aeronautical Science*, vol. 20, p. 29-42.
- Milne-Thomson, L.M. (1960) *Theoretical hydrodynamics*. New York: MacMillan Co., 4th Edition, 660 p.
- Smithsonian Meteorological Tables (1951) Publication 4014, Smithsonian Institution (R.T. List, preparer).
- Sokolnikoff, I.S. and R.M. Redheffer (1966) *Mathematics of physics and modern engineering*. New York: McGraw Hill, 2nd Edition.
- Stallabrass, J.R. (1957) Some aspects of helicopter icing. *Canadian Aeronautical Journal*, vol. 3, no. 8.
- Stallabrass, J.R. (1958) Canadian research in the field of helicopter icing. *Journal of the Helicopter Association of Great Britain*, vol. 12, no. 4, p. 3-40.
- Tribus, M. (1943) Development and application of heated wings. AFF TR4977, Addendum 1946.

```

ICE9
      *** CONTROL PROGRAM ***
      ** remember to scratch files before running **

      5 , FILE#1;"ICEFILE"
      15 FILE#2;"THERMOF"
      20 FILE#3;"DROPDIST"
      25 DIM U(30)
      30 DIM T(30)
      35 DIM C(30)
      40 DIM A(30)
      45 DIM F(30)
      50 DIM X(60)
      55 DIM Y(60)
      60 DIM E(60)
      65 DIM W(60)

      70 LIBRARY "PILOTLIB***;TEK10"
      75 DIM M(150)
      80 CALL "BAUD":M(),1200
      85 CALL "LIMITS":M(),"-1.5,-2.5+2.5
      90 CALL "PSIZE":M(),7.5,5.5
      95 ,  

      100 ,  

      105 ,  

      110 ,  

      115 LET X0= 7.5
      120 LET Y0=.5
      125 .  

      125 ** thermodynamic parameters appear in subprogram THERMO **
      130 PRINT "IF YOU WISH TO CHANGE ANY OF THE OBJECT PARAMETERS"
      135 PRINT "MODIFY DATA STATEMENT 300 ACCORDINGLY."
      140 PRINT
      145 PRINT "DO YOU WANT TO LOOK AT A SERIES OF VELOCITY PROFILES (INPUT -1) "
      150 PRINT "OR EXAMINE THE ENTIRE BLADE DISTRIBUTION (INPUT 0);"
      155 INPUT P1
      160 PRINT "DO YOU WANT TO SUPPRESS ALL GRAPHICAL OUTPUT."
      165 PRINT "(INPUT 1 = SUPPRESS);"
      170 INPUT P4
      175 IF P1>-1 THEN 195
      180 PRINT "INPUT THE VELOCITY PROFILE(S) (M/S)."
      185 MAT INPUT U
      190 PRINT
      195 PRINT "INPUT THE LIQUID WATER CONCENTRATION (KG/M^3)."
      200 PRINT "THE AMBIENT TEMPERATURE, AND (DEG. C), AND "
      205 PRINT "THE DROPLET RADIUS (CM) (INPUT 0 IF A".
      210 PRINT "DISTRIBUTION IS DESIRED)."
      215 INPUT W,T0,P2
      220 LET R= P2
      225 ,
      230 LET D= 2
      235 ,
      240 LET T1= 10
      245 ,
      250 LET T2= 300

      'D controls the time interval of the thermo balance - G3D must be integer
      'T1 sets the velocity increment size of the blade dist.
      'T2 sets the ** total model time **
```

```

255
260 LET J= 250/T1
265 IF P1>-1 THEN 285
270 LET J= NUM
275 LET T1= 0
280 LET U(0)= 0
285 FOR Z= 1 TO J
290 LET U0= U(Z)+T1*Z+U(0)
295 READ CO,A0,B0
300 DATA 20,1.27,1.26
305 LET A= A0/B0
310 LET B= 1
315 LET T= T0+ U0*2/2000
320
325 LET G3= 50
330
335
340 LET M= 0
345 LET E= 0
350 LET MO= 0
355 LET GO= 0
360 IF P2> 0 THEN 370
365 CALL "DROP DST":S,X0,Y0,U0,E,EO,R,W,X(),Y(),R(),W(),E(),N
370 CALL "PROFILE":M(),A,B,M,F,R,U0,T,FO,BO,P4,P2
375 CALL "TRAJECT":H(),X,Y,X0,Y0,U1,U,V1,U0,A,B,H0,R,LO,BO,P1,P4
380 CALL "COLL EFF":X,Y,X0,Y0,U1,U,V1,A,B,E,H0
385 IF E= 0 THEN 375
390 IF P2>0 THEN 410
395 CALL "DROP DST":S,X0,Y0,U0,E,EO,R,W,X(),Y(),R()
400 IF E= 0 THEN 375
405 LET S= 1
410 CALL "THERMO":E,U0,W,A,B,T,F,FO,CO,N,D,Q0,A0,BO,G0,T2,*2
415 IF P4= 1 THEN 430
420 IF P1= 0 THEN 430
425 CALL "PLOT T":M(),T,GO,T2,G3,D
430 LET GO= GO+D
435 LET G1= G1 + M*F
440 IF GO<G3 THEN 410
445 LET M= G1
450 LET G1= 0
455 LET MO= MO + M
460 IF GO = T2 THEN 485
465 LET G3= G3+ 50
470 IF F= 0 THEN 410
475 LET E= 0
480 GO TO 360
485 CALL "PROFILE":M(),A,B,M,F,R,U0,T,FO,BO,P4,P2
490 IF P2>0 THEN 500
495 PRINT #3:U0;"";"E(1)";"";"E(2)";"";"E(3)";"";"E(4)";"";"E(5)";"";"E(6)";"";"E(7)";"";"E(8)";"";"E(9)"
500 PRINT #1:U0;"";"E(1)";"";"E(2)";"";"E(3)";"";"E(4)";"";"E(5)";"";"E(6)";"";"E(7)";"";"E(8)";"";"E(9)"

' set up for-next loop parameters

' assign U0: current velocity of balde segment
' assign : heat capacity (joules/m^3deg C),maj. axis (cm),minor axis (cm)
'           ** A0 > B0 always: otherwise ellipse degenerates **
' dimensionless maj. axis length
' dimensionless minor axis length
' initialize T at recovery temperature

' G3 controls the time interval between updates of the
' coll. eff. (change 465 with G3)

' reset mass accreted during interval G3 for next profile
' reset collection efficiency for next velocity profile
' reset total mass accreted
' reset model time clock
' are we interested in a single droplet size?
' ask what kind of distribution, and pick up first droplet size
' have we calculated the coll eff for the drop yet?
' pick up next particle size
' if entire dist. scanned, then E = avg coll. eff., otherwise cycle back
' reset the droplet radius pointer so R(1) is up next

' plot new temperature (function of time for profile)
' increment model time clock D by amount of thermo balance time D
' increment the mass accreted by the amount accreted in time D
' if we haven't spent enough time in the thermo balance then go back
' reassign variables: let M = amount accreted in time G3 instead of D
' set total amount accreted in G3 to 0, for next cycle
' M keeps track of the mass accreted over the total model time
' check to see if we have run for the total model time yet
' calculate at what time the next profile update should occur
' if F=0 then no ice has accreted and we needn't draw a new profile
' the old E will be remembered unless we set it to zero

' plot last profile of sequence
' if a droplet dist. is not selected, then skip next line
' output velocity,temp.,ice thickness,col. eff.,and frac. accret. for pr

```

ICE9 (continued)

```
      RESET
      IF P#= 1 THEN 530
      IF NUM= 1 THEN 555
      CALL "MOVE":IN(),-1,2.5
      INPUT Q9
      NEXT Z
      IF P#= 1 THEN 570
      IF NUM= 1 THEN 555
      CALL "PT BLADE":IN(),T(),C(),A(),F(),A,R,T0,W,F2,$1,T2
      CALL "THERMOT":IN(),$2
      IF P2> 0 THEN 565
      CALL "PLOT D":IN(),R(),E(),W(),TO,U0,W,P1,N,$3
      CALL "FINISH":IN()
      END
      575
      580
      585
      590 SUB "TRAJECT": M(),X,Y,X0,Y0,U1,V1,U0,A,B,H0,R,L0,B0,P1,F4
      595      ' this subprogram essentially integrates newton's laws
      600      ' as applied to the droplet
      605      ** U0 in meters/sec   R in cm **
      610 CALL "MOVE":IN(),X0,Y0
      615 LET X=X0
      620 LET Y=Y0
      625 LET U1=U2=V2=0
      630 LET U1= -1
      635 LET T0= .1
      640 LET K= 1340**R**2*U0*100/B0
      645 LET L0= 1
      650 LET RO= 12.55*100*U0/R
      660 LET NO= .125 + L0*(K-.125)
      665      ** velocities and distances dimensionless **
      FOR T= 0 TO 1.00 STEP TO
      670 CALL "VELOCITY":X,Y,U,V,A,B,W,H1,Z,F,Q,B1
      675 LET RI= (((U1-U)*U0)^2+((V1-V)*U0)^2)^.5
      680 LET RO= 12.55*100*RI**R
      685 IF RO> 2 THEN 705
      690 LET D= 1 + 0.1024*RO^0.995
      695 LET RO= 725
      700 IF RO>21 THEN 720
      705 LET D= 1 + 0.115*RO^0.802
      710 LET T0= 725
      715 LET D= 1 + .189*RO^-.632
      720 LET U2= -D*(U1-U)*ABS(U1-U)*T0*U0/(R1*K0)
      725 LET V2= -D*(V1-V)*ABS(V1-V)*T0*U0/(R1*K0)
      730 LET U1= U1+U2
      735 LET V1= V1+V2
      740 LET X= X+ U1*T0
      745 LET Y= Y+ V1*T0
      750
```

(continued)

```

ICE9
755 IF P4= 1 THEN 775
760 IF P1=0 THEN 775
765 IF X> 5 THEN 775
770 CALL "LINE; H(),X,Y"
775 IF X>A THEN 860
780 LET Q0= BX/(A^2*(1-(X/A)^2)^.5)
785 IF Q0> ABS(V1/U1) THEN 810
790 IF ABS((X/A)^2+(Y/B)^2-.01)<.01 THEN 825
795 ,    ## trajectory missed target **
800 LET HO= 1
805 GO TO 865
810 LET I= (X/A)^2 + (Y/B)^2
815 IF I>1 THEN 860
820 IF ABS(V1/U1-Q0)>.1 THEN 845
825 LET HO= 2
830 ,    ## correct hit **
835 ,    ## trajectory within .1 arctan units of being tangent to profile **
840 GO TO 865
845 LET HO= 3
850 ,    ## particle hits target, but trajectory not tangent **
855 GO TO 865
860 NEXT T
865 SUBEND
870 ,
875 ,
880 ,
885 SUB "VELOCITY": X,Y,U,V,A,B,W,Hi,Z,P,Q,B1
890 ,    calculates stress velocity based on complex potential flow
895 ,    theory for an elliptical cylinder
900 LET HO= (X^2+Y^2)^.5
905 LET H= ATN(Y/X)
910 LET I= ABS(H1-H)
915 IF I< 3.14/2 THEN 925
920 LET W= W+ Z*I3.14159
925 LET Z= SGN(H)
930 LET H1=H
935 LET H= H + W
940 LET A0= ((X^2 - Y^2 - A^2+B^2)^2+4*X^2*Y^2)^.25
945 LET B0= (2*X*Y)/(X^2-Y^2-A^2+B^2)
950 LET BO= ATN(B0)
955 LET I= ABS(B1-BO)
960 IF I< 3.14/2 THEN 970
965 LET P= P+ I3.14159
970 LET Q= SGN(B0)
975 LET B1= BO
980 LET BO= -.5*(BO+P)
985 LET U= (HO*B1*COS(H-BO)/AO -A)/(A-B)
990 LET V= -B1*HO*SIN(H-BO)/(A-B)
995 SUBEND
1000 ,

```

ICEY (continued)

```
1005 '
1010 '
1015 SUB "COLL_EFF":X,Y,X0,Y0,U1,V1,A,B,E,H0
1020 ON H0 GO TO 1025:1055,1070
1025 '
1030 LET S= 1
1035 LET Y1= Y0*S*((1-(X/A)^2)^.5/Y)^S
1040 IF ABS(Y0-Y1)<.001 THEN 1060
1045 LET Y0= Y1
1050 GO TO 1110
1055 REM THIS BRANCH FOR CORRECT HIT
1060 LET E= Y0
1065 GO TO 1110
1070 REM THIS BRANCH FOR INC. HIT
1075 LET I=V1/U1
1080 LET T= ABS(A^2*B^2/(B^2+(A*I)^2)^.5)
1085 LET I0= B*(1-(T/A)^2)^-.5
1090 LET I= I0*I-Y-I*X
1095 LET Y1= Y0*(I0/I)
1100 IF ABS(Y1-Y0)<.001 THEN 1060
1105 LET Y0= Y1
1110 SUBEND
1115 '
1120 '
1125 '
1130 SUB "HTTRANS":N,A0,B0,U0,D
1135 ' THIS CORRELATION BASED ON HILPERT'S NUSSELT NUMBER
1140 ' CORRELATION FOR VARIOUS FLUIDS
1145 ' THIS HEAT TRANSFER RELATION
1150 ' SHOULD BE ADJUSTED TO ACCOUNT
1155 ' FOR THE FRONT SURFACE OF THE CYLINDER ONLY
1160 ' THIS HEAT TRANSFER CORRELATION
1165 ' GOOD ONLY FOR A/B < 2
1170 ' AND FOR RE > 4000
1175 LET R= 12.558U0100*A*B0
1180 LET C= (.5840/B0*.8)/1.3
1185 LET E= .8095
1190 LET K=.0239
1195 IF R> 40000 THEN 1225
1200 LET E= .618
1205 LET K= .174
1210 IF R > 40000 THEN 1225
1215 LET E= .464
1220 LET K= .615
1225 LET N= CAKRC'E
1230 LET N= NS.0248083.14159/4
1235 SUBEND
1240 '
1245 '
1250 '
```

'nusselt number based on hilpert's correlations  
'nusselt number converted directly to a (watts/meter of blade)

(continued)

```
ICE9   SUB *HTTRANS1:N,A0,B0,T0,U0,T,D
      THIS HEAT TRANSFER RELATION BASED ON BOSH'S CORRELATION
      IT INCORPORATES A FILM TEMPERATURE TO DETERMINE THE
      MASS DENSITY OF AIR, WHILE THERMAL COND.
      DATA AND HEAT CAPACITY DATA SHOULD BE CHANGED IF
      SIGNIFICANTLY DIFFERENT FROM VALUES AT 0 C.
      -UNITS IN MKS-
1290  LET P= 1014          ' SEA LEVEL PRESSURE
1295  LET F= (T0+T)/2 + 273.16
1300  LET K= .024
1305  heat transfer coefficient based on major axis length: watts/meter^2 des C
1310  LET H= 31.01*(U0)^-.56/(2*AO)^-.44*(P#273.16/(1014*F))^.56
1315  LET H= 1.12*H
1320  LET NO= H*(2*AO/100)/K
1325  LET N= H*D#3.14159*(AO+B0)/(4*A0+B0)
1330  SUBEND
1335  '
1340  '
1345  '
1350  SUB *THERMO:S,U0,W,A,B,T0,F,FO,CO,M,D,QO,A0,B0,G0,T5,*2
1355  REM TO INITIALIZE D
1360  REM THIS DOES NOT CONSIDER RADIAL FORCE EFFECTS
1365  REM NOR HEAT TRANSFER PARALLEL TO THE AXIS
1370  REM UNITS IN MKS
1375  DEF FNU(T)
1380  LET T= T+273.16
1385  LET T1= 373.16
1390  LET I= -7.9038*(T1/T)-1)+5.0281*.434294*LOG(T1/T)- 1.3816*10^(-7)*(10^(11.3444*(1-T/T1))-1)
1395  LET I= 1+8.1358*10^(-3)*(10^(-3.4915*(T1/T-1))-1)+.334294*LOG(1013.246)
1400  LET FNU= 10^-I
1405  FNEND
1410  DEF FNI(T)
1415  LET T2= 273.16
1420  LET T= T+273.16
1425  LET I= -9.0972*(T2/T-1)-3.5665*.434294*LOG(T2/T)
1430  LET I= 1+ .87679*(1-T/T2)+ .434294*LOG(6.1071)
1435  LET FNI= 10^-I
1440  FNEND
1445  READ R,C1,C2,F,EO,K
1450  DATA .8,1000,4180,
1455  DATA 1013,4.54,.024
1460  LET EO= FNU(T0)
1465  CALL *HTTRANS1:N,A0,B0,T0,U0,T,D
1470  LET H= W$#100*(B0/100)*D
1475  ON SGN(T)+2 GO TO 1635,1545,1480
1480  ** this branch for T > 0 **
1485  LET F= 0
1490  LET LO= 2500000
1495  LET E= FNU(T)
1500  LET IO= T-T0-R#U0^2/(2*C1) + .6*LO*(E-EO)/(F*C1)

      what is the vapor pressure of water over water at T degrees
      what is the vapor pressure of water over ice at T degrees ?
      what is the free stream vapor pressure ?
      what is the heat transfer coeff. (Watts/meter of blade ~ des c ~ D sec
      H is the amount of liquid water impinging per meter of blade
      what temperature regime are we interested in ?
      fraction accreted is zero for t>0
      heat of vaporization of liquid water at 0 deg. C
      what is the vapor pressure over the blade surface
```

(continued)

```
ICE9      LET I= M8C2*(T-T0-U0~2/(2*C2))
1505     LET Q0= -(N8I0+I)
1510     LET T1= (T*C0+Q0)/C0
1515     IF T1<0 THEN 1545
1520
1525
1530     LET T=0
1535     LET T= T1
1540     GO TO 1690
1545     ** this branch for T = 0 ***
1550     LET T= 0
1555     LET L0= 2500000
1560     LET L= 333600
1565     LET E= FNB(T)
1570     LET I0= -T0-R*U0~2/(2*C1)+.6*L0*(E-E0)/( C1*K)
1575     LET I= M8C2*(-T0-F*L/C2-U0~2/(2*C2))
1580     LET Q0= -(N8I0+I)
1585     LET F= F- Q0/(L*M)
1590     LET I1= ABS(F0-F)
1595     LET F0=F
1600     IF I1 >.001 THEN 1575
1605     IF F< 0 THEN 1480
1610
1615     IF F>1 THEN 1635
1620     LET C0= C0+F*M*C3
1625     GO TO 1690
1630
1635     ** this branch for T < 0 ***
1640     LET F=1
1645     LET L1= 2838000
1650     LET L= 333600
1655     LET C3= 2356
1660     LET E= FN1(T)
1665     LET I0= T-T0-R*U0~2/(2*C1) +.6*L1*(E-E0)/(F*K)
1670     LET I= M8C2*(T*C3/C2-T0-L/C2-U0~2/(2*C2))
1675     LET Q0= -(N8I0+I)
1680     LET C0= C0+M*C3
1685     LET T= -(T*C0+Q0)/C0
1690     IF (G0+2)<15 THEN 1735
1695     LET C9= -N8(A0+B0)*J3.14159/(4*100*D)*(T-T0-R*U0~2/(2*C1))
1700     LET E9= -N8(A0+B0)*J3.14159/(4*100*D)*J10 - C9
1705     LET S9= -N8(A0+B0)*J3.14159/(4*100*D)*C2*(T-T0)
1710     IF T> 0 THEN 1720
1715     LET S9= -N8(A0+B0)*J3.14159/(4*100*D)*C2*(T*C3/C2-T0)
1720     LET K9= M8(A0+B0)*J3.14159/(4*100*D)*U0~2/2
1725     LET L9= -I*(A0+B0)*J3.14159/(4*100*D)-S9-K9
1730     PRINT#2: U0;;,;IT;,;C9;,;E9;,;S9;,;K9;,;L9
1735     SUBEND
1740
1745
```

'what is the total heat transfer/meter of blade ?  
'how much does this heat transfer change the surface ? temperature ?  
'check to see that it did not make the temp go below zero  
(if it did, then go to t=0 branch

'L is the latent heat of freezing - Joules/kg  
'how much more ice can be frozen (or melted) with this excess q ?  
'if there is not enough q to freeze any ice the T goes below zero  
(in this case branch to the "above zero thermodynamics")  
'if there is more than enough q to freeze the water T drops below 0  
(in this case, branch to the "below zero thermodynamics"  
'the accretion changes the heat capacity of the blade  
\*\* exit subprogram \*\*\*

'heat of sublimation of ice at 0 deg. C  
'heat capacity of ice

'this is last time increment > output thermodynamic data:  
'convective heat transfer  
'evaporative heat transfer  
'heating due to influx of liquid water on blade (T >= 0)  
(T < 0)

'kinetic heating of droplets on impact  
'latent heat requirement to freeze water

ICE9 (continued)

```
1735 SUB *PROFILE*: M(),A,B,M,F,R,U0,T,P0,B0,P4,P2
1740 REM THIS CALCULATES AND PLOTS THE NEW PROFILE
1745 REN 'REINITIALIZE AFTER COMPLETION
1750 CALL "ICE.DEN":R,U0,T,P0,P2
1755 LET V= 1000000/(P0*100)
1760 LET A0= A$B0
1765 LET A0= 4$U/(B0^(2*$3.14159)) + A0
1770 LET A= A0/B0
1775 IF P4= 1 THEN 1835
1800 LET C= A/25
1805 CALL "MOVE":M(),0,1
1810 FOR X= 0 TO A STEP C
1815 LET Y= B$U-(X/A)^2)^.5
1820 CALL "LINE":M(),X,Y
1825 NEXT X
1830 CALL "MOVE":M(),X0,Y0
1835 SUBEND
1840 /
1845 /
1850 /
1855 SUB *ICE.DEN*: R:U0,T,P0,P2
1860 REM THE DENSITY FORMULA TAKES R IN CM
1865 IF P2= 0 THEN 1890
1870 IF T= 0 THEN 1890
1875 LET P0= .1104*(100000$R*U0/ABS(T))^-.76
1880 IF P0>.917 THEN 1890
1885 IF P0<.01 THEN 1895
1890 LET P0= .917
1895 SUBEND
1900 /
1905 /
1910 /
1915 /
1920 /
1925 /
1930 /
1935 SUB *PLOT T*:M(),T,G0,T2,63,D
1940 IF G0>0 THEN 1960
1945 CALL "MOVE":M(),0,-.5
1950 CALL "LINE":M(),0,-.5
1955 CALL "LINE":M(),4.5,-.5
1960 DEF FNY(T) = -1+(5+T)/10
1965 DEF FNX(G0) = 60360/(128*T2)
1970 LET X= FNX(G0)
1975 LET Y= FNY(T)
1980 CALL "MOVE":M(),X,Y
1985 CALL "LINE":M(),X,Y
1990 IF G0+D<63 THEN 2010
1995 CALL "MOVE":M(),FNX(G0),0
2000 CALL "LINE":M(),FNX(G0),-.5
'Put hacks on temp/time scale
```

ICE9 (continued)

```
2005 CALL "LINE":M(),T(),C(),A(),F(),A,R,TO,M,F2,$1,T2
2010 SUBEND
2015 '
2020 '
2025 '
2030 SUB "PT BLADE":M(),T(),C(),A(),F(),A,R,TO,M,F2,$1,T2
2035 REM THIS SUBPROGRAM PLOTS THE BLADE DISTRIBUTIONS
2040 DIM U(30)
2045 RESET #1
2050 INPUT #1:U,T,A,C,F
2055 LET K= K+1
2060 LET U(K)= U
2065 LET A(K)= A
2070 LET T(K)= T
2075 LET C(K)= C
2080 LET F(K)= F
2085 PRINT U(K),T(K),C(K),F(K)
2090 IF MORE#1 THEN 2050
2095 LET L1= 250
2100 CALL "CLEAR":M()
2105 CALL "CLEAR":M()
2110 CALL "LIMITS":M(),0,L1,-40,10
2115 CALL "PLIMITS":M(),1,6.5,25,5.25
2120 FOR N= 1 TO K
2125 CALL "LINE":M(),U(N),T(N)
2130 NEXT N
2135 CALL "LIMITS":M(),0,L1,-5,5
2140 CALL "PLIMITS":M(),1,6.5,3.75,4.75
2145 CALL "AXIS":M(),0,10,0,1
2150 CALL "LIMITS":M(),0,L1,0,1
2155 CALL "PLIMITS":M(),1,6.5,.75,1.75
2160 CALL "AXIS":M(),0,10,0,1
2165 FOR N= 1 TO K
2170 CALL "LINE":M(),U(N),C(N)
2175 NEXT N
2180 CALL "MOVE":M(),0,0
2185 FOR N= 1 TO K
2190 CALL "LINE":M(),U(N),F(N)
2195 NEXT N
2200 DEF FM(A)= A-1
2205 CALL "PLIMITS":M(),1,6.5,2.25,3.25
2210 CALL "AXIS":M(),0,10,0,1
2215 CALL "LIMITS":M(),0,L1,0,3
2220 CALL "PLIMITS":M(),1,6.5,2.25,5.25
2225 FOR N= 1 TO K
2230 CALL "LINE":M(),U(N),FNA(A(N))
2235 NEXT N
2240 CALL "LIMITS":M(),0,250,0,1
2245 CALL "PLIMITS":M(),0,5,5,0,5,5
2250 CALL "MOVE":M(),100,.8
```

ICE9 (continued)

```
2235 PRINT "Temperature Distribution."
2240 CALL "MOVE":M(),130,.1
2245 PRINT "Velocity (cm/sec)."
2250 CALL "MOVE":M(),250,.1
2255 PRINT " "
2260 CALL "MOVE":M(),250,.1
2265 PRINT " "
2270 CALL "MOVE":M(),250,.1
2275 PRINT " "
2280 CALL "MOVE":M(),230,.7
2285 PRINT T = $T0: (C).
2290 CALL "MOVE":M(),230,.685
2295 PRINT " "
2300 CALL "MOVE":M(),230,.655
2305 PRINT "1WC=";W;"ks/m^3".
2310 IF F2= 0 THEN 2330
2315 CALL "MOVE":M(),230,.625
2320 PRINT "R = ";R*10000;" (microns)"
2325 GO TO 2355
2330 CALL "MOVE":M(),230,.625
2335 PRINT "Droplet Dist. Selected"
2340 CALL "MOVE":M(),230,.595
2345 PRINT "Ave Coll Eff Disp."
2350 CALL "MOVE":M(),100,.82
2355 CALL "MOVE":M(),0,.850
2360 PRINT " "
2365 PRINT
2370 PRINT
2375 PRINT "T (deg C)."
2380 PRINT
2385 PRINT " "
2390 PRINT " "
2395 CALL "MOVE":M(),100,.56
2400 PRINT "Ice Thickness Distribution"
2405 CALL "MOVE":M(),0,.57
2410 PRINT " "
2415 PRINT "Thickness"
2420 PRINT " "
2425 PRINT " "
2430 CALL "MOVE":M(),100,.37
2435 PRINT "Collection efficiency and Fraction"
2440 CALL "MOVE":M(),100,.34
2445 PRINT "Accreted Distributions"
2450 CALL "MOVE":M(),0,.3
2455 PRINT " "
2460 CALL "MOVE":M(),230,.73
2465 PRINT "Model Time:$T2; sec"
2470 SUBEND
2475 REM
2480 REM
2485 REM
2490 SUB "DROP DST":D,X0,Y0,U,E,O,R,W,X(),Y(),R(),W(),E(),N
2495 REM THIS SUB. KEEPS TRACK OF DROPLET IMPACTS
2500 REM SIZE, INITIAL STARTS, ECT.
```

ICEP (continued)

```
2505 IF D > 0 THEN 2785
2510 FILE03: 'DROPDIST.
2515 PRINT *INPUT 1,2,OR 3, IF A GAUSSIAN, ERLANG, OR*
2520 PRINT *SPECIFIED DISTRIBUTION IS DESIRED. ;
2525 INPUT A
2530 PRINT *INPUT DROPLET DATA IN MICRONS*
ON A GO TO 2540,2605,2680
2535 REM THIS SAMPLES THE GAUSSIAN BETWEEN +/- 2 SIGMA OF THE MEAN
2540 REM THIS INCLUDES 95 PERCENT OF THE DISTRIBUTION
2545 REM THIS INCLUDES 95 PERCENT OF THE MEAN, VARIANCE, AND TOTAL # OF DROPLET SIZES*
2550 PRINT *INPUT M,S2,N
2555 INPUT M,S2,N
2560 LET S= S2^.5
2565 FOR K= M-245 TO M+245 STEP 4*S/(N-1)
2570 IF K<0 THEN 2595
2575 LET D= D+1
2580 LET P(D)= EXP(-(K-M)^2/(2*S2))/(2*3.14159*S2)^.5
2585 LET R(D)= K
2595 NEXT K
2600 GO TO 2715
2605 REM THIS BRANCH FOR ERLANG PDF
2610 REM THIS SAMPLES FROM RO TO RO + 2*MEAN
2615 PRINT *INPUT ERLANG ORDER, K*(1/L)= <MEAN>, THE DISTRIBUTION*
2620 PRINT *START RADIUS, AND THE TOTAL # OF DROPLET SIZES*;
2625 INPUT K,M,RO,N
2630 LET L= K/M
2635 LET U(0)=V(1)= 1
2640 LET U(1)= 2
2645 LET U(2)= 3*U(2)
2650 FOR I= M/10 TO M STEP (2*M-M/10)/(N-1)
2655 LET D= D+1
2660 LET R(D)= I+RO
2665 LET P(D)= L^K*I^-(K-1)*EXP(-I*L)/U(K-1)
2670 NEXT I
2675 GO TO 2715
2680 REM THIS BRANCH FOR SPECIFIED DISTRIBUTION
2685 PRINT *INPUT # OF DROPLET SIZES IN SPECTRUM*
2690 INPUT N
2695 PRINT *INPUT DROPLET RADIUS, AND PERCENTAGE (BY NUMBERS) CONTRIBUTION*
2700 FOR K= 1 TO N
2705 INPUT R(K),P(K)
2710 NEXT K
2715 LET I= P(1)*R(1)^3+P(2)*R(2)^3+P(3)*R(3)^3+P(4)*R(4)^3+P(5)*R(5)^3
2720 LET I= I+P(6)*R(6)^3+P(7)*R(7)^3+P(8)*R(8)^3+P(9)*R(9)^3
2725 LET H= W/(4*3.1415*I/3)
2730 PRINT *DROPLET SIZE LWC*
2735 FOR K= 1 TO N
2740 READ X(K),Y(K)
2745 DATA 10,.7
2750 LET W(K)= 4*3.14159*R(K)^3*P(K)*H/3
2755 PRINT R(K),W(K)
```

(continued)

```
1CE9
2760 PRINT #31R(K)";",":M(K)
2765 LET R(K)=R(K)*.0001
2770 RESET
2775 NEXT K
2780 LET D= 1
2785 LET X(D-1)= X0
2790 LET Y(D-1)= Y0
2795 LET X0= X(D)
2800 LET Y0= Y(D)
2805 LET R= R(D)
2810 LET E(D-1)= E
2815 LET EO= EO + E*W(D-1)/W- E(D)*W(D)/W
2820 LET E= 0
2825 IF R(D)>0 THEN 2835
2830 LET E= EO
2835 LET D= D+1
2840 SUBEND
2845 REM
2850 REM
2855 REM
2860 SUB "PLOT D::M(),R(),W(),TO,JO,W,P1,N,+.3
2865 REM THIS SUB FOR PLOTING DROPLET DIST.
2870 RESET #3
2875 PRINT "*"
2880 INPUT Q
2885 CALL "CLEAR":M()
2890 CALL "LIMITS":M():0,100,0,3
2895 CALL "PLIMITS":M(),2,2,.75,.475
2900 CALL "MOVE":M(),50,2,5
2905 PRINT "Droplet Distribution"
2910 CALL "MOVE":M(),55,2,4
2915 PRINT "T = ":#T0
2920 CALL "MOVE":M(),55,2,35
2925 PRINT " "
2930 CALL "MOVE":M(),55,2,25
2935 PRINT "U = ":#U0": /sec."
2940 CALL "MOVE":M(),55,2,2
2945 PRINT " "
2950 FOR D= 1 TO N
2955 INPUT #3: R(D),W(D)
2960 CALL "LINE":M(),R(D),1000*W(D)
2965 NEXT D
2970 INPUT #3:U0,E(1),E(2),E(3),E(4),E(5),E(6),E(7),E(8),E(9)
2975 CALL "MOVE":M(),0,0
2980 FOR D= 1 TO N
2985 CALL "LINE":M(),R(D),E(D)*W(D)*1000
2990 NEXT D
2995 IF MORE#3 THEN 2970
3000 CALL "AXIS":M(),0,10,0,25
3005 CALL "PLIMITS":M(),1,5,25,4,25
```

(continued)

```
ICE9      CALL "MOVE":N),0,2
3010      PRINT " 1WC.
3015      CALL "MOVE":N),0,1.8
3020      PRINT "(3/8*3).
3025      CALL "MOVE":N),40,0
3030      PRINT "Droplet Radius (microns)      100.
3035      CALL "PLIMITS":M(),1.8*5.8,.75,4.75
3040      CALL "MOVE":N),0,2.95
3045      PRINT "3"
3050      CALL "MOVE":N),0,1.95
3055      PRINT "2."
3060      CALL "MOVE":N),0,.95
3065      PRINT "1.
3070      SUBEND
3075      SUBEND
3080      SUB "PLOT M":M(),I(),U()
3085      PRINT "
3090      INPUT A
3095      CALL "LIMITS":M(),0,230,0,5
3100      CALL "PLIMITS":M(),1.5,5,1,5.5
3105      CALL "MOVE":N),3.65
3110      PRINT "Total Mass Accretion (g/cm)*
3115      CALL "AXIS":N(),0,2,0,10
3120      FOR Z= 1 TO 27
3125      IF U(Z)= 0 THEN 3140
3130      LET I(Z)= I(Z)*1000/100
3135      CALL "LINE":M(),U(Z),I(Z)
3140      NEXT Z
3145      CALL "FINISH":M()
3150      SUBEND
3155      "
3160      "
3165      "
3170      SUB "THERMOPT":N(),#2
3175      INPUT A
3180      DIM U(30),T(30),C(30),E(30),S(30),K(30),L(30)
3185      RESET #2
3190      INPUT #2:U,T,C,E,S,K,L
3195      LET N= N+1
3200      LET U(N)= U
3205      LET T(N)= T
3210      LET C(N)= C
3215      LET E(N)= E
3220      LET S(N)= S
3225      LET K(N)= K
3230      LET L(N)= L
3235      PRINT U,T,C,E,S,K,L
3240      IF MORE#2 THEN 3190
3245      CALL "CLEAR":M()
3250      CALL "CLEAR":N()
3255      LET L1= 250
```

'L1 sets the maximum velocity of the plot

ICE9 (continued)

```
3260 LET Y0= -5
3265 LET Y1= 6
3270 CALL "LIMITS":M(),0,L1,Y0,Y1
3275 CALL "PLIMITS":M(),1,P5,.5-.5
3280 CALL "AXIS":M(),0,10,0,0,1
3285 FOR K= 1 TO N
3290 CALL "LINE":M(),U(K),C(K)
3295 NEXT K
3300 CALL "MOVE":M(),U(K),C(K)
3305 PRINT "C"
3310 CALL "MOVE":M(),0,0
3315 FOR K= 1 TO N
3320 CALL "LINE":M(),U(K),E(K)
3325 NEXT K
3330 CALL "MOVE":M(),U(K),E(K)
3335 PRINT "."
3340 CALL "MOVE":M(),0,0
3345 FOR K= 1 TO N
3350 CALL "LINE":M(),U(K),S(K)
3355 NEXT K
3360 CALL "MOVE":M(),U(K),S(K)
3365 PRINT "S"
3370 CALL "MOVE":M(),0,0
3375 FOR K1= 1 TO N
3380 CALL "LINE":M(),U(K1),K(K1)
3385 NEXT K1
3390 CALL "MOVE":M(),U(K1),K(K1)
3395 PRINT "K"
3400 CALL "MOVE":M(),0,0
3405 FOR K= 1 TO N
3410 CALL "LINE":M(),U(K),L(K)
3415 NEXT K
3420 CALL "MOVE":M(),U(K),L(K)
3425 PRINT "."
3430 CALL "LIMITS":M(),0,1,0,1
3435 CALL "MOVE":M(),35,.95
3440 PRINT "Icins Thermodynamics (watts/meter^2)"
3445 CALL "MOVE":M(),7,.9
3450 PRINT "C= convective heat transfer"
3455 CALL "MOVE":M(),7,.87
3460 PRINT "S= evaporative heat transfer"
3465 CALL "MOVE":M(),7,.84
3470 PRINT "S= influx of a due to droplet"
3475 CALL "MOVE":M(),.7,.81
3480 PRINT "super-coolins"
3485 CALL "MOVE":M(),.7,.78
3490 PRINT "k= kinetic heatings of droplets"
3495 CALL "MOVE":M(),.7,.75
3500 PRINT "from impaction"
3505 CALL "MOVE":M(),.7,.72
```

ICE9 (continued)

```
'Y0 sets minimum on heat transfer scale
'Y1 sets maximum on heat transfer scale
3510 PRINT "l= latent heat requirement to"
3515 CALL "MOVE":M(),7,.69
3520 PRINT "freeze accreted water"
3525 CALL "MOVE":M(),4,-Y0/(Y1-Y0)-.04
3530 PRINT "velocity (m/sec)"
3535 CALL "MOVE":M(),0,1
3540 PRINT Y1
3550 CALL "MOVE":M(),0,.1
3555 PRINT V0
3560 PRINT V0
3565 subend
```

A facsimile catalog card in Library of Congress MARC format is reproduced below.

Ackley, S.F.

Computer modeling of atmospheric ice accretion / by S.F. Ackley and M.K. Templeton. Hanover, N.H.: U.S. Cold Regions Research and Engineering Laboratory; Springfield, Va.: available from National Technical Information Service, 1979.

iii, 39 p., illus.; 27 cm. (CRREL Report 79-4.)

Prepared for Directorate of Military Programs, Office, Chief of Engineers by Corps of Engineers, U.S. Army Cold Regions Research and Engineering Laboratory.

Bibliography: p. 21.

- 1. Cold regions.
  - 2. Computerized simulation.
  - 3. Control.
  - 4. Deicing systems.
  - 5. Drops.
  - 6. Ice.
  - 7. Ice formation.
  - 8. Mathematical models.
  - 9. Test methods.
  - 10. Clouds.
- I. United States. Army. Corps of Engineers. II. Army Cold Regions Research and Engineering Laboratory, Hanover, N.H.  
III. Series: CRREL Report 79-4.

\*U.S. GOVERNMENT PRINTING OFFICE: 1979 - 601-060/360